Helsinki Medical Imaging Center

Helsinki University Central Hospital

University of Helsinki

Helsinki, Finland

ASSESSMENT OF CARDIAC FUNCTION WITH MAGNETIC RESONANCE IMAGING AND A THREE-DIMENSIONAL SEGMENTATION METHOD

Description of Mulibrey nanism cardiopathy and effects of endurance training on cardiac function

Sari Kivistö

Academic dissertation

To be presented, with the assent of the Medical Faculty of the University of Helsinki, for public examination in Lecture Room 12, Main building of the University of Helsinki, on the 20th of May, 2005, at 12 noon.

Helsinki 2005

Supervisors

Docent Kirsi Lauerma

and

Docent Pauli Hekali

Helsinki Medical Imaging Center

University of Helsinki

Reviewers

Docent Johanna Kuusisto

Department of Cardiology

University of Kuopio

and

Professor Jaakko Hartiala

Department of Clinical Physiology and Nuclear Medicine

University of Turku

Opponent

Docent Pekka Niemi

Department of Diagnostic Radiology

University of Turku

ISBN 952-91-8614-2 (paperback)

ISBN 952-10-2431-3 (PDF)

Helsinki University Printing House

Helsinki 2005

To Jaakko and Jussi…

TABLE OF CONTENTS

ABSTRACT

The general purpose of this work was to evaluate the capacity of magnetic resonance imaging (MRI) for assessing cardiac function, particularly diastolic function.

Study objectives

Studies I and II: To describe characteristic features of Mulibrey nanism (MUL) with cardiac MRI. To assess volumes of all cardiac chambers, thickness of the pericardium and left ventricular (LV) mass, and to differentiate between constrictive pericarditis and restrictive cardiomyopathy.

Study III: To assess the effect of endurance training on the early diastolic global and regional LV myocardial relaxation and systolic myocardial function with mitral flow velocity mapping, myocardial four-chamber tagging and cine MRI.

Study IV: To describe an automated three-dimensional (3-D) segmentation method for all four cardiac chambers.

Methods

We examined 31 MUL patients and 16 controls to describe MUL cardiopathy (I, II). In addition, we investigated 14 subjects before and after a three-month training period to describe the effectiveness of endurance training on LV function (III). We combined the segmentation results of 25 subjects; 16 subjects from Study III (=14 subjects+2 excluded subjects who underwent only one MRI) and 9 control subjects from Study II to build a statistical atlas of cardiac chambers, thus providing the basis for automated segmentation tools (IV). MRI studies were approved by the Human Research Committee of Helsinki University Central Hospital and performed at Helsinki Medical Imaging Center with a 1.5 T magnetic resonance scanner. In Studies I and II, the volumes and functions of all four cardiac chambers were assessed. In Study III, LV function was evaluated with mitral flow velocity mapping, myocardial four-chamber tagging, and cine MRI.

Results

In Studies I and II, the thickness of the pericardium was normal (<3.5 mm) in all MUL patients. Both left and right ventricular end-diastolic volumes were smaller in MUL patients than in controls ($p<0.008$). Although LV systolic function was preserved in patients, concentric LV hypertrophy and restrictive filling were present. The right ventricular ejection fraction was reduced ($p<0.001$). Both atria were mildly enlarged, and cyclic volume changes in the atria were reduced ($p<0.05$).

In Study III, mitral flow velocity mapping revealed that the time to peak early filling shortened after training, indicating more rapid global early myocardial relaxation. Early diastolic myocardial relaxation in the septum and in the LV lateral wall increased. Regional longitudinal tagging analysis showed that after training myocardial relaxation was significantly enchanced in the basal septum ($p<0.05$) and contraction in the apical septum ($p<0.05$).

In Study IV, a movement correction algorithm and a statistical 3-D atlas for all four cardiac chambers were built using short-axis and four-chamber views.

Conclusions

According to our MRI results, MUL cardiopathy was characterized by concentric LV hypertrophy and restrictive filling due to both myocardial and pericardial abnormalities. Both atria were mildly enlarged and cyclic volume changes were reduced. In addition RV ejection fraction was reduced. All these features suggested an elevated afterload due to LV diastolic impairment (I, II).

Physiological LV hypertrophy was found after three months of endurance training in healthy subjects. According to mitral flow velocity mapping and four-chamber tagging analysis, global and regional LV early diastolic relaxation improved (III).

With the movement correction algorithm the edges both in atria and ventricles became more continuous. An automated 3-D segmentation method for measurement of both atria and ventricles was developed by combining information on standard short-axis and four-chamber images (IV).

2. LIST OF ORIGINAL PUBLICATIONS

This thesis is based on the following original articles, which are referred to in the text by their Roman numerals:

I. Kokki S, Lauerma K, Kupari M, Lipsanen-Nyman M, Hekali P. Assessment of Mulibrey nanism cardiopathy with functional magnetic resonance imaging. Magnetic Resonance Materials in Physics, Biology and Medicine 2000; 11: 84-86.

II. Kivistö S, Lipsanen-Nyman M, Kupari M, Hekali P, Lauerma K. Cardiac Involvement in Mulibrey Nanism: Characterization with Magnetic Resonance Imaging. Journal of Cardiovascular Magnetic Resonance 2004; 6: 645-652.

III. Kivistö S, Perhonen M, Holmström M, Lauerma K. Diastolic tagging indicates the effectiveness of training on myocardial relaxation. Scandinavian Journal of Medicine Science in Sports (Submitted).

IV. Lötjönen J, Kivistö S, Koikkalainen J, Smutek D, Lauerma K. Statistical shape model of atria, ventricles and epicardium from short- and long-axis MR images. Medical Image Analysis 2004; 8: 371-386.

The publishers of the original articles have kindly given their permission for these papers to be reprinted. Some unpublished material is also presented.

3. LIST OF ABBREVIATIONS

2-D	two-dimensional
3-D	three-dimensional
4-D	four-dimensional
ECG	electrocardiogram
FA	flip angle
FISP	fast imaging with steady-state free precession
GRE	gradient echo
LA	left atrium / atrial
LV	left ventricle / ventricular
MR	magnetic resonance
MRI	magnetic resonance imaging
MUL	Mulibrey nanism
RA	right atrium / atrial
RF	radio frequency
ROI	region of interest
RV	right ventricle / ventricular
SE	spin echo
T1	longitudinal relaxation
T2	transverse relaxation
TE	time to echo
TR	time of repetition

4. INTRODUCTION

The most common methods for studying cardiac anatomy and function are echocardiography (=cardiac ultrasound), computed tomography, and magnetic resonance imaging (MRI). Two-dimensional (2-D) echocardiography is a real-time imaging modality with rapid image acquisition and excellent spatial and temporal resolution. The availability of the method is good, its cost is low and, if necessary, it can be performed at patient's bedside. The technique has limitations in acoustic windows, restricting its use in patients with advanced chronic pulmonary disease, patients who have undergone open-chest cardiac surgery and obese patients (Kuhl *et al.*, 2004).

Diastolic and systolic images can be produced in an anatomically optimized orientation from multi-detector row spiral computed tomography data with a retrospective electrocardiographic (ECG) gating technique. Rotation speeds of the x-ray tube and detector rows have increased and costs of the study are reasonable. Moreover, multi-detector row computed tomography has the advantage of breath-hold data acquisition and is suitable for patients with pacemakers and implanted defibrillators. Drawbacks of the technique are radiation exposure and limited temporal resolution (Juergens *et al.*, 2004).

MRI is an accurate and reproducible method to measure atrial and ventricular volumes, function and ventricular mass. Compared with other non-invasive imaging modalities, MRI can more accurately assess the right side of the heart and pericardium. However, MRI is not suitable for patients with implanted defibrillators, ferromagnetic clips, pacemakers, arrhythmias or claustrophobia. Time resolution is not as good as in echocardiography, but is markedly improved with the newer imaging techniques (Sprung, 2005). Most prosthetic heart valves are not ferromagnetic, although the prosthetic material itself causes a localized image artefact (Edwards *et*

al., 2000). Advantages of MRI are absence of radiation, good reproducibility and ability to assess three-dimensional (3-D) volumes of atria and ventricles directly, without any geometric assumptions (Pluim *et al.*, 1997, Pattynama *et al.*, 1995, Pattynama *et al.*, 1993).

Modern cardiac MRI protocols should include analysis of all cardiac chambers during systole and diastole to assess early indicators of cardiac disease. Although cine MRI is potentially useful in assessing cardiac function, its routine use in clinical setting has been limited by its long manual post-processing time (Lötjönen, 2003b, Lötjönen, 2004a). A clinical application for automated 3-D segmentation of all cardiac chambers is therefore needed.

5. REVIEW OF THE LITERATURE

5.1. BASIC PRINCIPLES OF CARDIAC MAGNETIC RESONANCE IMAGING

MRI is an ideal non-invasive tool for imaging and diagnosing myocardial and pericardial diseases. It provides anatomical information with high spatial resolution and differentiates between the blood pool and the lung in any plane without radiation exposure. MRI is suited to assess both pericardial thickness and internal cardiac anatomy. It is a practical method for distinguishing constrictive pericarditis from restrictive cardiomyopathy. In addition, MRI gives valuable information about the right side of the heart (Masui *et al.*, 1992, Frank and Globits, 1999, Soulen, 1991, Higgins, 2000).

5.1.1. Signal on magnetic resonance images

The signal in MRI is obtained from tissue protons in water and lipids. Protons possess an intrinsic spin, and since they are positively charged, they generate a small magnetic field. In tissues, the proton spins are randomly oriented, and their magnetic fields cancel each other. When the patient is placed into the MR imager and exposed to an external field, the magnetic moment of the spin results in the preferred orientation, and if forced into a less convenient position is correlated with consumption of energy. Since the preferred position of a parallel alignment shows a higher population, a macroscopic magnetization is built up. Since a radio frequency (RF) field is applied at the same frequency as the precession of tissue protons, the protons absorb energy. When the excitation RF pulse is turned off, the excited protons return to equilibrium and release their absorbed energy at the same resonant frequency, producing a MR signal. There are two relaxation processes, which can be used to characterize substances and influence contrast in an image. First,

the macroscopic magnetization (i.e. longitudinal magnetization) will get back into original position. The time needed for this process is called longitudinal relaxation (T1) time. Second, as the protons move around their environment, they experience varying magnetic fields due to their neighbours. This causes a spread of resonant frequencies, corresponding to a dephasing of magnetization in the (rotating) transverse plane. The time needed for this process is called transverse relaxation (T2) time. Both values are tissue-specific. T1 and T2 weighting of the MR sequence are dependent on timing of the sent excitation RF pulses and collection of the MR signal from the tissue (= readout). The time between the repeated excitation RF pulses is called time of repetition (TR). The time from the excitation pulse to readout is called time to echo (TE) (Westbrook and Kaut, 1995).

5.1.2. Cardiac triggering

The greatest challenges in the acquisition of cardiac MR images or cine display have been the motion artefacts caused by breathing, and artifacts from myocardial motion and blood flow. Breath-hold imaging is the approach used most widely for avoiding respiratory-related displacement of the heart.

Right and left ventricular (LV) filling show normal respiratory variation. With inspiration, systemic venous return into the right atrium (RA) increases, and right ventricular (RV) diastolic filling volumes are 20% higher than end-expiratory values. Left atrial (LA) filling does not increase with inspiration since pulmonary venous return is not affected significantly by respiratory change (Otto, 1995). All sections should be acquired at the same end-expiration phase to minimize the effects of respiratory variation.

MRI systems with respiratory navigator guided sequences reduce the number of artefacts resulting from chest wall motion and eliminate the need for breath-holding (Paelinck *et al.*, 2002).

ECG gating synchronizes cardiac imaging at preselected intervals during the cardiac cycle. Data are collected in gates or time windows at synchronized intervals to produce gated images throughout the phases of the cardiac cycle (Greenberg and Sandhu, 1999). Prospective cardiac gating initially developed for cardiac synchronization of MR data acquisition can be used for any type of MRI sequence. The duration of image acquisition must be less than or equal to the duration of the shortest R-R interval. In practice, this usually means that the last 10 - 20% of diastole is not acquired. Retrospective gating was developed for synchronization of rapid repetitive cine acquisition to the cardiac cycle. In retrospectively gated cine, images are acquired continuously while ECG signals are recorded and subsequently sorted according to their position in the cardiac cycle, thus enabling the entire cardiac cycle to be efficiently imaged (Feinstein *et al.*, 1997). Because prospective as well as retrospective gating requires data acquisition over multiple heart beats, irregular heart rhythms (e.g. atrial fibrillation) substantially diminish image quality (Sondergaard *et al.*, 1999). Arrhythmia rejection is a new imaging method that is useful, if the heart rate of a patient is very irregular. It directs the system to reject data, if a R-peak is not within the RR-window (Paelinck *et al.*, 2002).

5.1.3. Gradient echo cine imaging

The basic gradient echo (GRE) technique uses a single RF excitation pulse of 10 – 90^{o} to produce an echo signal. Reversal of the magnetic field gradients rephases the spins and produces an echo at time of TE. Generally, short TRs and TEs are employed. The TR values used for GRE do not compensate for the dephasing process, and therefore, the appearance of GRE images is influenced by T2*, the sum effect of magnetic field distortions that cause loss of transverse magnetization. With a given TR, the use of a large flip angle (FA) and short TE sequences produces predominantly

T1-weighted images, whereas the use of a small FA and long TE yields predominantly T2*-weighted images. Because ECG-triggered GRE MRI allows the use of short TR and short TE, it is suitable for assessing the function and volumes of all four cardiac chambers (Greenberg and Sandhu, 1999). Gradient imaging produces ”bright blood images”, where blood appears white and the myocardium grey. Flow disturbances, such as those found with regurgitate jets or septal defects, produce flame-shaped areas of signal loss that correspond to intensely turbulent jet regions (Pettigrew *et al.*, 1999).

TR can be shortened to several milliseconds with such fast GRE techniques as turbo fast low angle shot, which uses very small FA and short TR. The major improvement in speed results from acquiring not one but multiple lines of image resolution per heart beat for each phase in the cine sequence. A single cine image series can be acquired during free breathing in 1-2 min and during a breath-hold in 10 - 20 seconds (Pettigrew *et al.*, 1999, Haase, 1990).

5.1.4. Fast imaging with steady-state free precession technique

A resent technique, true FISP (=fast imaging with steady-state free precession) uses the steady state of residual transverse magnetisation in addition the steady state of longitudinal magnetisation. When TR is much less than T2, the image signal is proportional to the T2/ T1 ratio. Because blood has significantly higher T2/T1 ration than myocardium, it is possible to diffentiate the blood, myocardium and epicardial fat excellently. The use of true FISP has been limited until recently, as it is susceptible to magnetic field inhomogeneities and requires very short TRs (Sprung, 2005). True FISP is greatly superior to fast low angle shot cine imaging and may become in the future gold standard acquisition technique for volume and mass studies (Earls *et al.*, 2002, Pennell, 2002, Moon *et al.*, 2002).

The following protocol is designed to obtain volumetric data from the atria and ventricles.
An axial scout can be defined from the sagittal and coronal scout images and is acquired according to the definition of a two-chamber view. The scan plane is set to the axial scout through the apex, the middle of the mitral valve, and the LA. The four-chamber view is set perpendicular to the two-chamber view (Alfakih *et al.*, 2004b). Cine images in the four-chamber planes can be obtained for the volumetric study of the atria (Järvinen *et al.*, 1994a, Järvinen *et al.*, 1994b). A single basal short-axis slice is positioned in the four-chamber view parallel to the plane of the atrioventricular ring at the back of the ventricles, with the two anchor points being the extreme rear of the RV and LV myocardium. Cine images in the short-axis planes can be obtained for the volumetric study of ventricles (Alfakih *et al.*, 2003b, Lorenz *et al.*, 1999, Pennell, 2002, Bellenger *et al.*, 2000a) (Figure 1).

5.1.5. Phase contrast or velocity-encoded cine techniques

Flow-encoded phase shifts result from application of bipolar magnetic field gradients, which are composed of two lobes with opposite signs. When the first lobe is applied, the spins of the stationary and moving tissues begin to accumulate phase. Immediately after the first lobe, the second lobe is applied, and the stationary protons lose their phase and accumulate a net phase of zero. Blood that moves during the time between these two gradients experiences unequal positive and negative gradients, and therefore accumulates a net phase shift (Szolar *et al.*, 1996, Hartiala *et al.*, 1994).

The flow measurement plane should be set exactly perpendicular to the direction of flow through the atrioventricular valve, to avoid underestimation of maximum velocity. If the approximate velocity selected is too low, aliasing degrades the information. Higher velocity spins, by contrast,

are displayed incorrectly and cannot be differentiated from flow in the opposite direction(Szolar *et al.*, 1996). Accurate determination of functional changes requires a temporal resolution of less than 40 ms (frame rate over 25/s)(Fujita *et al.*, 1993, Hartiala *et al.*, 1993).

The phase shift, which is proportional to the velocity, is displayed as pixel intensity on the phase map image. Motion in the positive direction along the flow-encoding axis will appear as bright pixels. Flow in the opposite direction appears as dark pixels, and stationary tissue appears grey. When performing cardiac gating, which is mandatory for pulsate flow assessment, two (positive and negative) flow-encoded acquisitions are acquired as interleaved pairs at each point of the cardiac cycle. To suppress the background noise, the phase-encoded pixel intensities may be multiplied by magnitude image, which is a by-product of the interleaved phase difference technique. The resulting images are called “flow” images (Szolar *et al.*, 1996) (Figure 2).

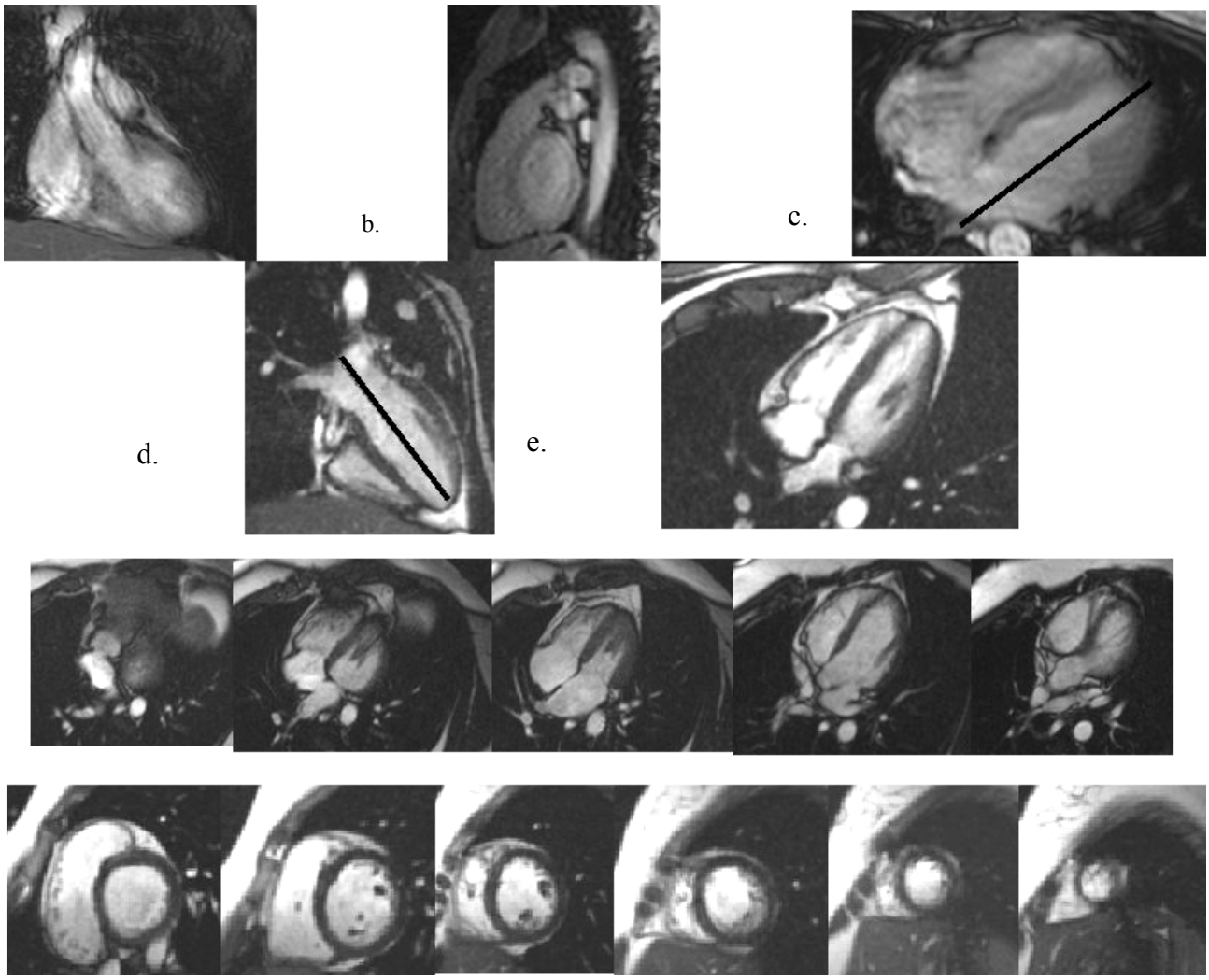

Figure 1. **Demonstration of imaging protocol in assessment of volumetric data of both atria and ventricles from cine image.**

a. Coronal scout image.

b. Sagittal scout image.

c. Axial scout image. The scan plane is set through the apex and the left atrium.

d. Two chamber view. The scan plane is set through the apex and the left atrium.

e. Four-chamber view.

f. Cine images in the four-chamber planes for the volumetric study of the atria.

g. Cine images in the short-axis planes for the volumetric study of the ventricles.

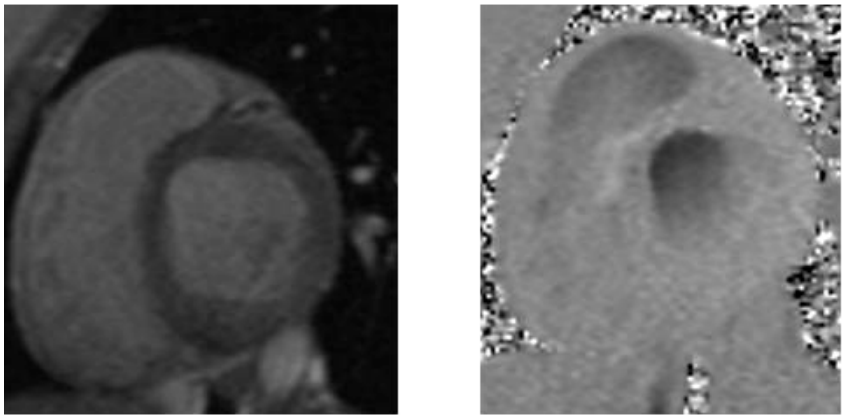

a. b.

Figure 2. Velocity-encoded cine images. Anatomical (a) and flow-encoded (b) images through the mitral valve.

The slice is positioned in the midway between the end-systolic and end-diastolic locations of the mitral valve and angulated parallel to it.

5.1.6. Myocardial tagging

Myocardial tagging is a technique to label or "tag" the myocardium by selective saturation prepulses in specific myocardial regions in planes perpendicular to the imaging plane. The tags appear as black lines (absence of signal from these protons), and deform with the tissue. Systolic myocardial deformation is assessed by depositing the tags as early as possible after detection of the QRS complex to capture motion through systole. In assessment of diastolic tagging, tag deposition and the imaging sequence are delayed until end-systole (Reichek, 1999) (Figure 3).

5.1.7. Spin echo imaging

With spin echo (SE) technique, an initial excitation pulse (90^o RF pulse) is applied to tilt the spins around the axis of the excitatory magnetic field. Longitudinal magnetization is reduced and transverse magnetization is generated but starts to disappear rapidly because of spin dephasing. After a time period of one half of TE, a refocusing pulse (180^o RF pulse) is applied, to produce a coherent signals, and after another one half of TE an echo is produced. The combination of selected TR and TE determines whether images have T1- or T2-weighting. T1-weighted SE images are acquired with a combination of short TR and short TE. T2-weighted SE images are acquires with a combination of long TR and long TE. Faster turbo SE technique has replaced conventional SE imaging. (Nitz, 1999)

Turbo SE imaging collects multiple echoes to fill the raw data matrix. Each echo has a different phase encoding. The possible reduction in measurement time is directly proportional to the number of echoes used. Although the technique is much faster than conventional SE, its limitation is in the loss of small details. On the other hand, decreased scan time reduces respiratory movement artefacts (Pettigrew *et al.*, 1999) (Figure 4).

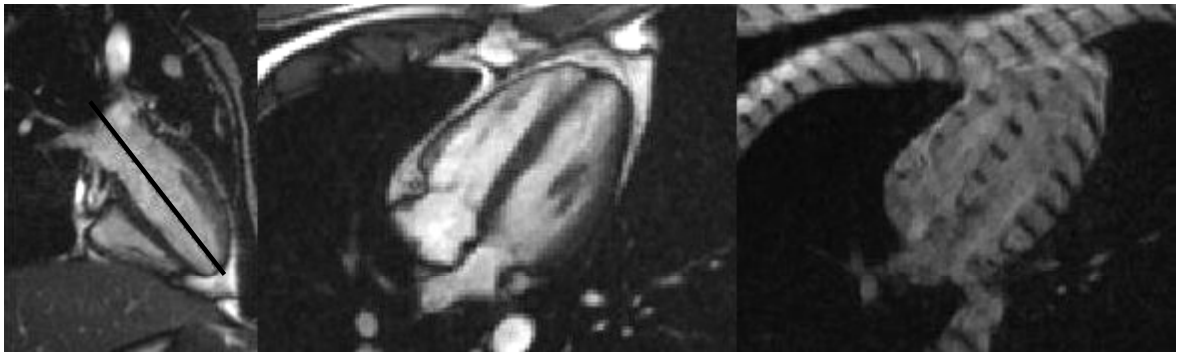

Figure 3. Left ventricular four-chamber tagging image.

The four-chamber view for tagging is set perpendicular to the two-chamber view.
Images are labelled with cross-section lines at a 90^{o} angle to the interventricular septum.

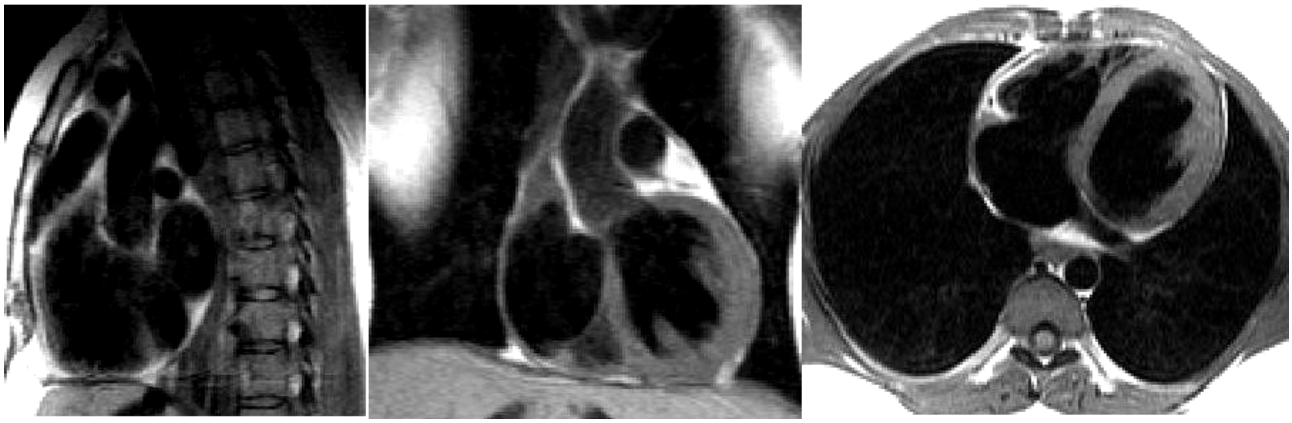

a. b. c.

Figure 4.

Turbo spin echo T1-weighted images were obtained for measurement of pericardial thickness in Mulibrey nanism patient.

a. Sagittal plane, b. Coronal plane, c. Axial plane.

5.2. MAGNETIC RESONANCE IMAGE ANALYSIS

3-D volumes of all four cardiac chambers can be assessed from MRI images without any geometric assumptions (Friedrich, 2000, Pluim *et al.*, 1997). MRI is characterized by high accuracy and reproducibility in measurements of both LV and RV morphology and function, especially if the ventricle is morphologically abnormal (Soulen, 1991, Pattynama *et al.*, 1993, Semelka *et al.*, 1990, Allison *et al.*, 1993, Pattynama *et al.*, 1994, Pattynama *et al.*, 1995). A major advantage in MRI as compared with echocardiography, is a better visibility to the right side of the heart and to the apex, and accurate assessment of pericardial thickness (Di Cesare, 2001). MRI is superior to 2-D echocardiography, which seems to overestimate LV mass and underestimate LV volumes (Alfakih *et al.*, 2003a, Pluim *et al.*, 1997, Bellenger *et al.*, 2000a, Bottini *et al.*, 1995, Katz *et al.*, 1988, Rehr *et al.*, 1985). 3-D echocardiography is reported to be superior to the 2-D technique, particularly in the assessment of deformed hearts, as the volumes are calculated from 3-D data sets by summing of the areas of multiple parallel levels without geometric assumptions. The method is, however, less reproducible and more operator- and patient-dependent than cardiac MRI (Alfakih *et al.*, 2004b, Friedrich, 2000).

The volume changes in the ventricles and atria during systole and diastole describe the cardiac function. Manual volumetric tracing of all four cardiac chambers throughout the cycle is possible but is so time-consuming that much important functional data may be overlooked. Semiautomated and automated segmentation algorithms are valuable in shortening the post-processing time in assessing chamber volumes. Hitherto, these computer algorithms have concentrated on detection of endocardial and epicardial ventricular boundaries from 2-D images (van der Geest *et al.*, 1997). Earlier studies have applied a 3-D shape model for the LV (Mitchell *et al.*, 2002), but a 3-D shape model for the whole heart has not yet been developed. Using a 3-D model as a quantitative

segmentation tool, would yield more accurate quantitative information than 2-D techniques (Lötjönen, 2004b, Lötjönen *et al.*, 2003, Lötjönen, 2004a, Lötjönen, 2003b, Mitchell *et al.*, 2002).

5.2.1. Cine magnetic resonance image analysis

Both RV and LV volumes can be determined from short-axis cine images. RV short-axis volume data are available as a by-product of LV short-axis volume acquisition. For the actual short-axis RV data, the stacks of short-axis slices should be planned so that they are parallel to the tricuspid valve. Extra care is therefore needed when analysing the most basal slice. In the outflow part of the RV, the portion of the volume above the pulmonary valve is excluded. In the inflow part, the volume of the RA is excluded. The RA wall is thin and untrabeculated (Alfakih *et al.*, 2004b, Lorenz *et al.*, 1999). The aortic outflow region below the valve plane is included at end-diastole for determination of LV volume (Figure 5).

Both atrial volumes can be determined from long-axis cine images. The inlets of the superior and inferior vena cava and the coronary sinus must be excluded from the RA volume. The pulmonary vein inlets must be excluded from the LA volume. The atrioventricular groove is used to define the atrioventricular border (Järvinen *et al.*, 1994a, Järvinen *et al.*, 1994b).

The gold standard for measurement of ventricular volumes has been to apply Simpson's rule to short-axis cine MR images and is summarized by the equation: $V=\Sigma^{n}A\ (S+G)$, where V is the chamber volume, A is the area of the lumen of the slice, S is the slice section thickness, G is the gap thickness and n is the number of slices encompassing the ventricle. The use of end-diastolic and end-systolic images allows measurement of diastolic and systolic volumes of all four cardiac chambers. As no geometric assumptions are used, the summation of the slice volumes through the

chamber is equal to the total volume (Soldo *et al.*, 1994, Greenberg and Sandhu, 1999, Lorenz *et al.*, 1999, Bellenger *et al.*, 2000b).

The ventricular end-diastolic short-axis image is the image with the largest LV cavity area, and the end-systolic image is the image with the smallest LV cavity area. Time-volume curves can be generated by acquiring data points throughout the cardiac cycle (Soldo *et al.*, 1994, Greenberg and Sandhu, 1999, Kudelka *et al.*, 1997) (Figure 6).

LV mass can be obtained by applying Simpson's rule to the same 3-D data set obtained to evaluate the ventricular volumes. LV mass can be measured from either end-systolic or end-diastolic images. The total ventricular mass is determined by subtracting the chamber volume from the total ventricular volume (= chamber + muscle), with 1.05 g/ml as the density factor for the myocardium. Papillary muscles are usually excluded from LV end-diastolic volume and included in LV mass (Pluim *et al.*, 1997). The volume of papillary muscles represents 6.5$\pm$1.3% of the end-diastolic volume (van der Geest *et al.*, 1997).

With an automated 3-D segmentation method, all acquired images at different planes can be used for chamber volumetry. Using a combination of two- and four-chamber views, the boundary between atria and ventricles and the shape of the apical parts of the ventricles can be determined more accurately. In addition to 3-D volumetry, four-dimensional (4-D) information reflected as time-volume changes can be assessed from all four cardiac chambers (Figure 7). With this information, small functional failures of the heart can be identified, and the effect of training and treatment assessed (Sievers *et al.*, 2004).

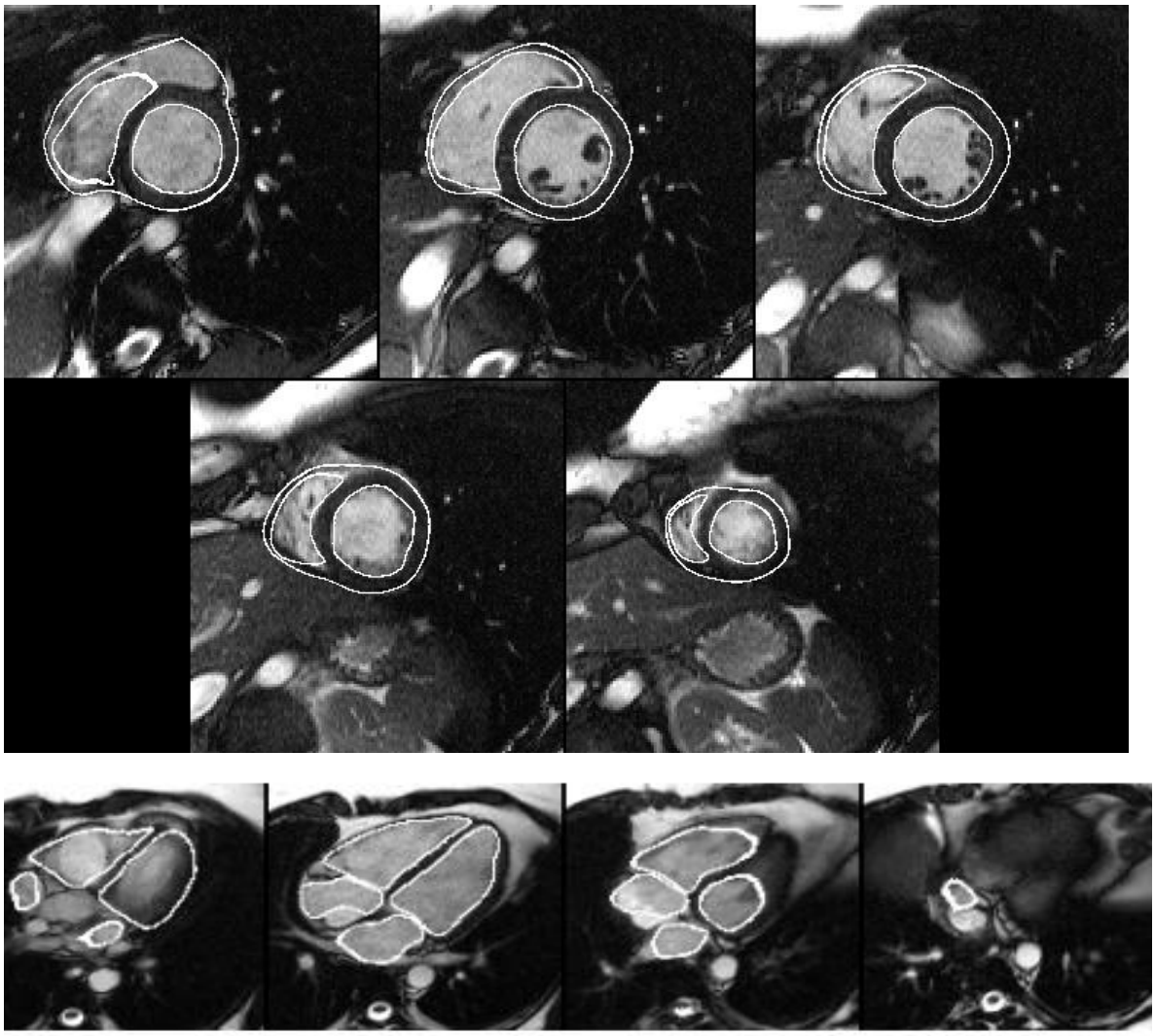

Figure 5. Automated segmentation of both atria and venticles for one subject

The contours on the ventricular and atrial volumes are from the same triangulated surface.

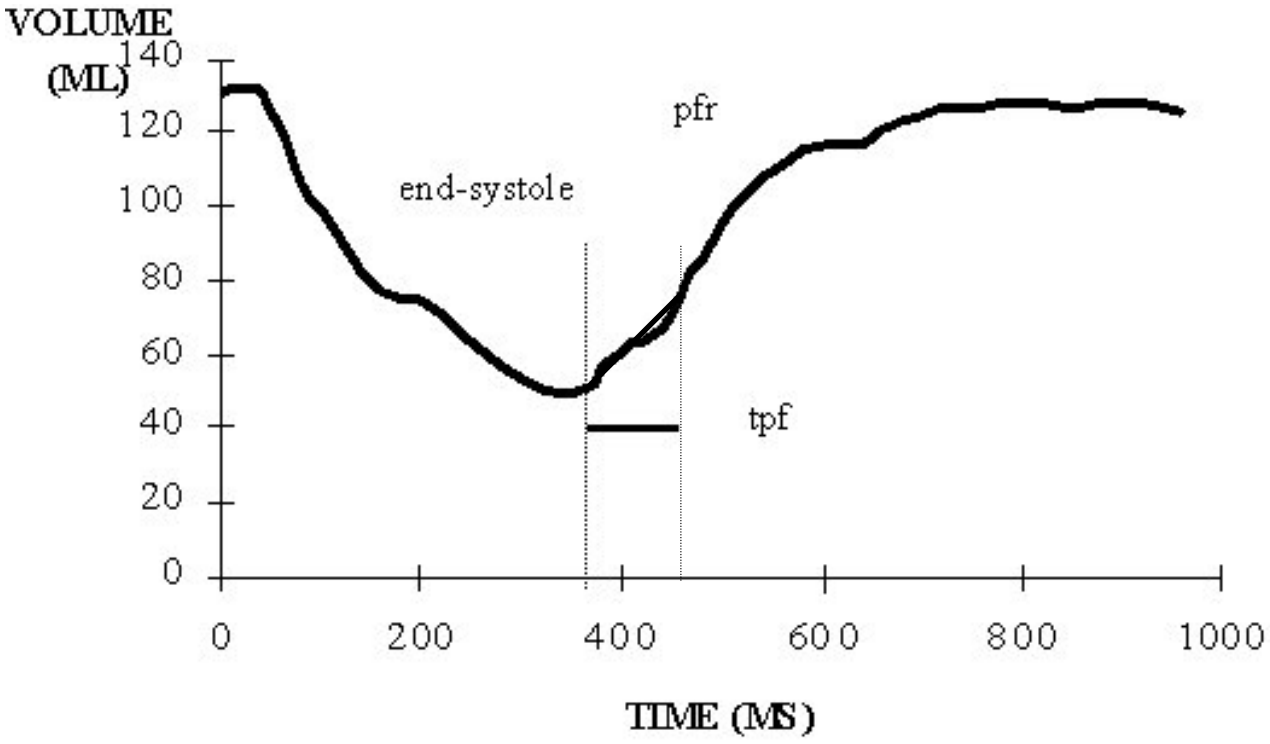

Figure 6. Time-volume curve of the left ventricle determined after R-wave

pfr = absolute peak filling rate of the left ventricle

tpf = time from end-systole to occurrence of peak rate of ventricular diastolic filling

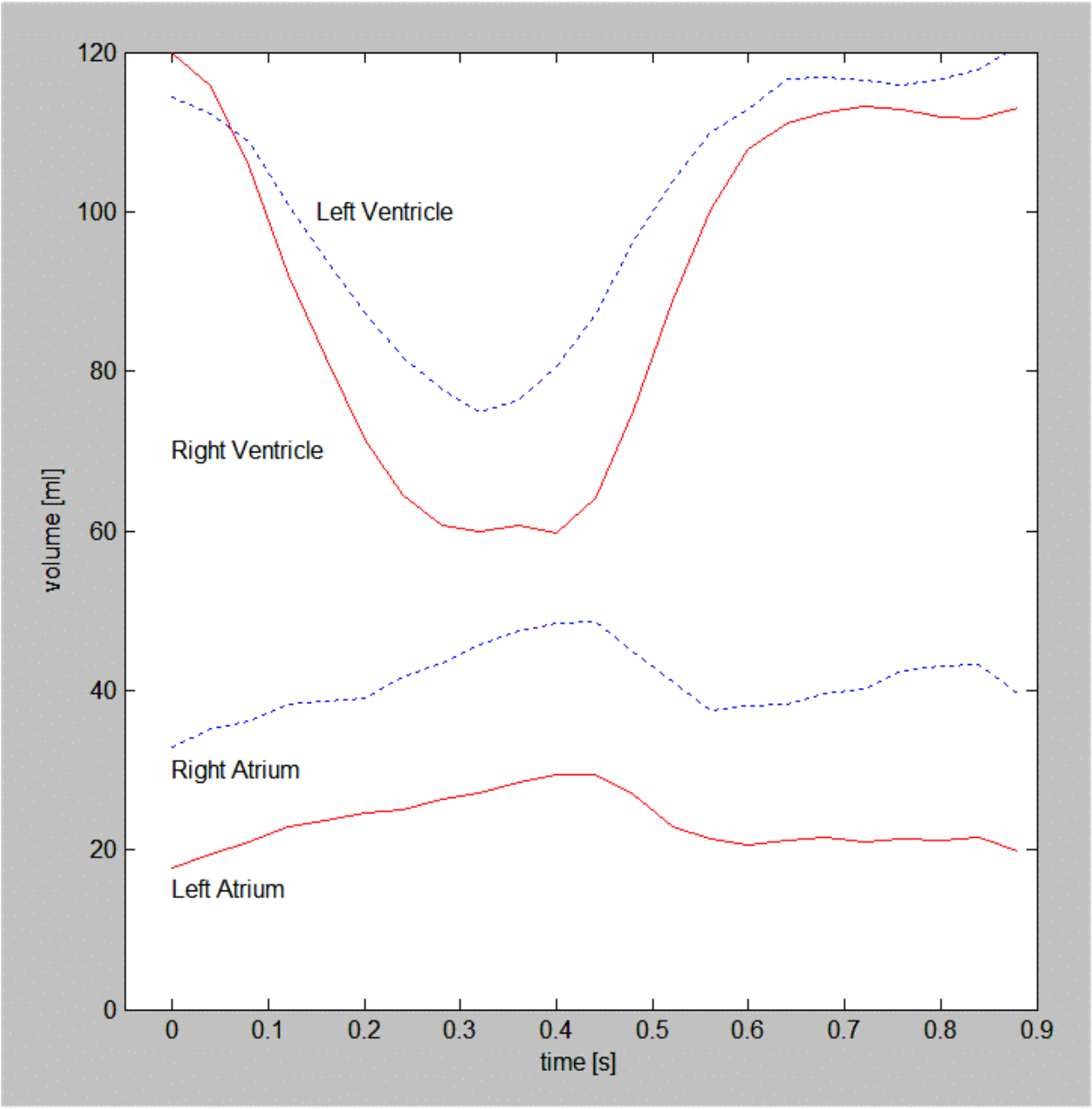

Figure 7. Automated four-dimensional segmentation of all four cardiac chambers

5.2.2. Phase contrast or velocity-encoded cine image analysis

To determine the flow profile or the flow volume a region of interest (ROI) is drown at the location of the atrioventricular valve. The ROI is superimposed on subsequent images throughout the cardiac cycle and can be adjusted if any change in size or location occurs. The averaged velocity in the ROI measures on the phase image is then multiplied by the cross-sectional area to generate a flow volume measurement (mean blood flow = mean flow x cross-sectional area).

Mitral and tricuspid inflow is characterized by two positive peaks (early ventricular diastole and atrial contraction). Diastolic function parameters derived from the inflow curves; the time to peak early filling, the peak early filling rate, the deceleration time of the early diastolic wave, the duration of the early diastolic wave (Paelinck *et al.*, 2002) and the early filling volume (Pluim *et al.*, 1998) can be determined. (Figure 8).

Although peak velocities and volume flow of early and atrial filling waves through both atrioventricular valves have been measured accurately with MR velocity encoding, the low temporal resolution of the conventional sequences does not allow to measure the isovolumic relaxation time reliably (Paelinck *et al.*, 2002, Hartiala *et al.*, 1993).

5.2.3. Myocardial tagging data analysis

Tagged cardiac MR images give information on regional myocardial function. The motion pattern of the myocardium can be observed visually by cine series display. Torsion patterns and ventricular regions with abnormal contraction and relaxation can be identified. At the moment, the benefits of quantitative tagging analysis are limited, and the programs difficult to use. The simplest method is

to track the side-to-side separation of tag lines in a single plane. The change in distance between line pairs at end-diastole and end-systole represents unidimensional shortening or elongation of the myocardium in one direction. Unidimensional tag analyses lack assessment of rotation and translation of tag lines. Ongoing image processing research may increase the level of automatization in analysis of tagged images. After segmentation of all landmarks, a displacement map of myocardial tissue can be generated, and from this, regional torsion angle and strain rates, both circumferential and radial, can be derived. By combinating of two orthogonal stacks of tagged images, these parameters can be derived in three dimensions (rotation, radial displacement, and translation) (Reichek, 1999, Paelinck *et al.*, 2002) (Figure 9).

5.2.4. Spin echo image analysis

ECG-gated T1-weighted SE images can be used for evaluating morphology of the heart and great vessels since the contrast between the myocardium, ventricular cavities, epicardial fat and pericardium is good. These images demonstrate pericardial thickening with sufficient reliability and predictive accuracy to diagnose or exclude pericardial constriction. This has important value in differentiating constrictive pericarditis from restrictive cardiomyopathy (Masui *et al.*, 1992, Hartnell *et al.*, 1996). Pericardial thickness should be measured from turbo SE T1-weighted images, because SE imaging does not overestimate thickness, as do GRE sequences in the presence of pericardial fluid and calcification (Soulen, 1991, Masui *et al.*, 1992).

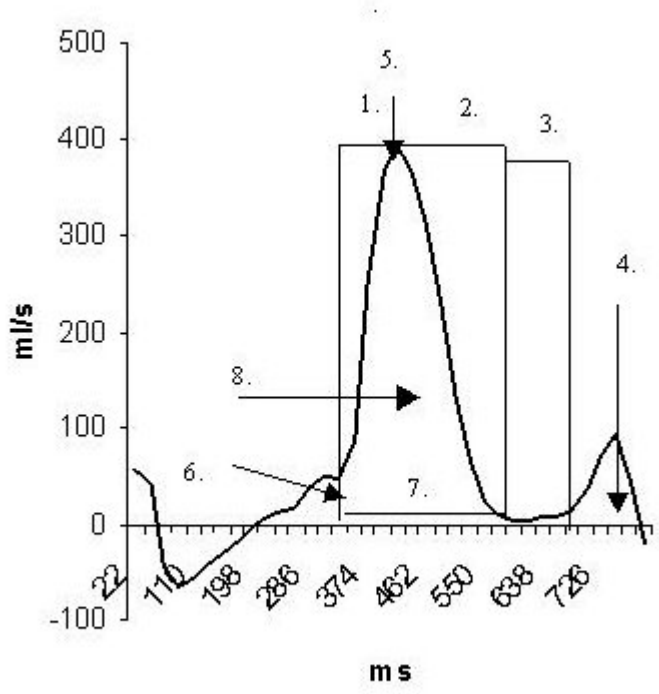

Figure 8. Magnetic resonance velocity inflow curve across the mitral valve

1. Time to peak early filling = time between the early diastole and the time point at which peak early filling rate occurs (ms)2. Deceleration time of early diastolic wave (ms)

3. Diastase (ms)

4. Atrial filling volume = area under second peak (ml)

5. Peak early filling rate = maximal flow rate of first peak (ml/s)

6. Beginning of early diastole

7. Duration of early diastole (ms)

8. Early filling volume = area under first peak (ml)

9a.

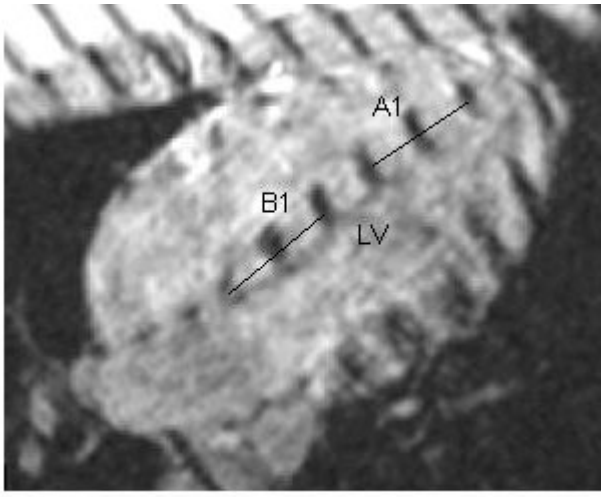

9b.

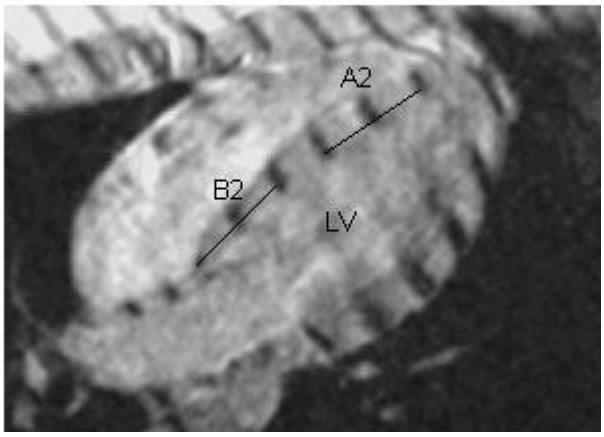

Figure 9a. MR four-chamber tagging image in early diastole

LV = left ventricle
B1 = early diastolic distance between three basal tag lines in the septum
A1 = early diastolic distance between three apical tag lines in the septum

Figure 9b. MR four-chamber tagging image in end-diastole

LV =left ventricle
B2 = end-diastolic distance between three basal tag lines in the septum
A2= end-diastolic distance between three apical tag lines in the septum

Diastolic myocardial relaxation fraction in the base (%) = [(B2-B1) / B2] * 100

Diastolic myocardial relaxation fraction in the apex (%) = [(A2-A1) / A2] * 100

5.3. MAGNETIC RESONANCE IMAGING OF DIASTOLIC FUNCTION

5.3.1. Normal ventricular diastolic function

Diastolic filling consists of four phases: 1) isovolumic relaxation, 2) early diastolic rapid filling (= E-wave), 3) diastase and 4) late diastolic filling (= A-wave) (Greenberg and Sandhu, 1999, Matsuda *et al.*, 1983) (Figure 10). The pattern of RV filling is similar to LV diastolic filling (Andrew, 2003). The major differences between RV and LV filling are that RV maximal velocities are lower because the tricuspid annulus is larger than the mitral annulus, reciprocal respiratory variation exists in the RV filling, and the RV diastolic filling period is slightly shorter (Otto, 1995).

Isovolumic relaxation is the time from the closure of the aortic and pulmonary valves to the opening of the atrioventricular valves. After the aortic and pulmonary valves close, ventricular pressure falls rapidly, and when the pressure falls below atrial pressure, the atrioventricular valves open (Otto, 1995, Greenberg and Sandhu, 1999). A very short isovolumic relaxation time is a reliable sign of elevated LA pressure, whereas abnormal prolongation indicates the combination of ventricular disease with normal or mildly elevated filling pressure (Gibson and Francis, 2003).

In the rapid filling phase that follows the opening of the atrioventricular valves, blood flows from the atria to the ventricles. The rate and time of the filling phase are limited by ventricular loading conditions and systolic function. LV filling and distension are dependent on RV hemodynamics (Greenberg and Sandhu, 1999).

Diastase is the time during which the pressure between the atrium and the ventricle equalizes. There is little movement of blood between the chambers. The duration of diastase is heart rate-dependent, being longer at slow heart rates and shorter or entirely absent at faster heart rates (Otto, 1995).

The late diastolic filling phase is caused by atrial contraction during atrial systole. In normal individuals, approximately 20% of ventricular filling occurs during atrial systole (Matsuda *et al.*, 1983, Otto, 1995).

Diastole encompasses the time period during which the myocardium loses its ability to generate force and to shorten, returning to an unstressed length and force. Diastolic dysfunction occurs when these processes are prolonged or incomplete (Zile and Brutsaert, 2002a).

-

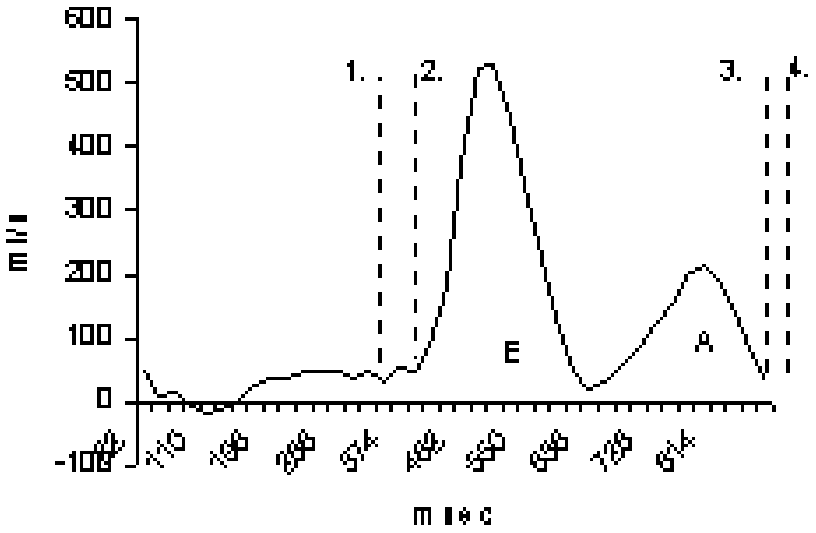

Figure 10. **Normal ventricular diastolic function**

1. Aortic valve closing click
2. Mitral valve opening click
3. Mitral valve closing click
4. Aortic valve opening click

Isovolumetric relaxation = time from closure of the aortic valve to the opening of the mitral valve

E-wave = early diastolic rapid filling phase

Diastase = time during which the pressure between the atrium and ventricle equalizes

A-wave = atrial contraction during atrial systole

5.3.2. Pathophysiology of diastolic dysfunction

Many myocardial diseases alter the LV diastolic function before any changes can be observed in systolic function (Lorenz *et al.*, 2000, Takemoto *et al.*, 1992). Diastolic dysfunction explains up to 40% of congestive heart failure in patients with normal systolic function (Libonati, 2000).

Diastolic dysfunction is a condition in which abnormalities in function are present during diastole. Diastolic function is determined by the passive elastic properties of the LV and by the process of active relaxation. Abnormal passive elastic properties are generally caused by a combination of increased myocardial mass and collagen. The effects of impaired active myocardial relaxation can further stiffen the ventricle. As a result, LV diastolic pressure in relation to volume increases. In diastolic heart failure, stroke volume and cardiac output are reduced despite a normal ejection fraction (Andrew, 2003). A small increase in central blood volume or an increase in venous tone or arterial stiffness can cause a substantial increase in LA and pulmonary venous pressure and may result in acute pulmonary oedema (Zile and Brutsaert, 2002a, Redfield *et al.*, 2003, Zile and Brutsaert, 2002b, Aurigemma and Gaasch, 2004, Zile *et al.*, 2004).

In the normal ageing process, diastolic function is impaired in a manner similar to changes seen in clinical disorders leading to LV diastolic dysfunction. Early diastolic ventricular filling diminishes, whereas atrial contribution to LV filling becomes increasingly prominent. This age-related decline in diastolic function is associated with a decrease in LV relaxation due to structural and functional alterations of the myocardium caused by the ageing process of the heart (Takemoto *et al.*, 1992, Nottin, 2004, Kitzman *et al.*, 2002, Henriksen *et al.*, 1999, Fonseca *et al.*, 2003).

Diagnosis of diastolic heart failure requires signs or symptoms of heart failure, a normal or slightly reduced ejection fraction (≥45%) and evidence of abnormal LV relaxation, filling, diastolic distension or diastolic stiffness (Mandinov *et al.*, 2000, Zile and Brutsaert, 2002a).

Diastolic dysfunction is usually associated with hypertension, atrial fibrillation, diabetes, coronary artery diseases, renal diseases and dilated cardiomyopathy. These conditions have been linked to myocardial hypertrophy, interstitial fibrosis and ischaemia which can prolong relaxation and increase passive myocardial stiffness (Burkhoff *et al.*, 2003, Redfield, 1930). The following section (i.e. 5.3.3.) describes the common conditions associated with diastolic dysfunction.

5.3.3. Diseases causing diastolic dysfunction

5.3.3.1. Left ventricular hypertrophy

LV hypertrophy is a common finding, and its presence supports, but is not required for a diagnosis of diastolic heart failure (Zile *et al.*, 2004). As a consequence of chronic pressure overload, the LV responds by developing hypertrophy to normalize wall tension. Hypertrophy, together with altered passive elastic properties, leads to diastolic dysfunction. LV hypertrophy is usually due to hypertension or aortic stenosis. The predominant abnormality is impaired relaxation, resulting in a pattern of a reduced early diastolic rapid filling phase and an enhanced atrial contribution to filling (Lorenz *et al.*, 2000, Lipton and Coulden, 1999).

Hypertrophic cardiomyopathy is an autosomal dominant disease characterized by myocardial hypertrophy and myocyte disarray with a variable clinical expression (Sipola *et al.*, 2003b). More than 150 different mutations in 11 genes encoding sarcomeric proteins have been identified

(Jääskelainen *et al.*, 2004). Diastolic dysfunction is a very early phenomenon in hypertrophic cardiomyopathy, even preceding LV hypertrophy (Nagueh *et al.*, 2003).

5.3.3.2. Restrictive cardiomyopathy

Restrictive cardiomyopathy is characterized by primary abnormalities in diastolic ventricular function, with a normal to slightly reduced ejection fraction. Restrictive abnormality of ventricular function can result from myocardial disease (infiltration of the myocardium by fibrosis or other tissue) or endomyocardial fibrosis. Differential diagnosis is usually made by cardiac catheterization combined with endomyocardial biopsy (Frank and Globits, 1999).

Diagnostic findings in restrictive cardiomyopathy include dilated atria, inferior vena cava and hepatic veins, whereas ventricles have normal or reduced volume. The RV can be elongated and narrow, and the septum sigmoid-shaped (Soulen, 1991). Restrictive cardiomyopathy is frequently complicated by mitral or tricuspid regurgitation (Frank and Globits, 1999).

5.3.3.3. Pericardial effusions or constriction

Normal pericardial thickness is usually 1-2 mm and appears on MRI as a low intensity signal between the mediastinal and subepicardial fat. The pericardium consists of two layers. The visceral pericardium is continuous with the epicardial surface of the heart. The parietal pericardium is a dense, fibrous structure that is closely apposed to the pleural surfaces laterally and isolates the heart from the mediastinum, lungs and pleural spaces anatomically. The pericardial space normally contains a small amount of fluid (5-10 ml according to echocardiography studies (Otto and Pearlman, 1995) and 10-50 ml according to MRI studies (Krombach *et al.*, 2002)). Pericardial

effusion or constriction can cause impaired filling of the ventricles during diastole. Pericardial effusion can be transudative, exudative or haemorrhagic (Soulen, 1991).

In constrictive pericarditis, the pericardial thickness generally exceeds 3.5-4 mm (Masui *et al.*, 1992). Morphologically, pericardial thickening is a manifestation of fibrous pericarditis. It may involve either the parietal or the visceral leaflet and can cause adhesions between them. The aetiology of progressive pericardial fibrosis leading to constrictive pericarditis can be infectious pericarditis, tuberculosis, connective tissue disease, neoplasm or trauma.

5.3.3.4. Mulibrey nanism cardiopathy

Mulibrey (Muscle-Liver-Brain-Eye) nanism (MUL) is an autosomal recessive disease with prenatal-onset growth failure and multiorgan dystrophy, including cardiovascular, skeletal, hepatic, endocrine and ophthalmologic abnormalities (Perheentupa, 1973). Worldwide, approximately 100 patients have been identified 80 of who are Finnish (Lipsanen-Nyman *et al.*, 2003). The causative mutations have recently been lokalized to the TRIM37 gene, which encodes a RING-B-box-Coiled-coil zinc protein residing in peroxisomes (Avela *et al.*, 1997, Avela *et al.*, 2000).

MUL is a rare diastolic disorder with combined pericardial and myocardial disease.
The clinical spectrum of MUL cardiopathy extends from severe congestive heart failure unresponsive to pericardiectomy in early childhood to asymptomatic LV hypertrophy and filling impairment in adulthood. Constrictive pericarditis has been regarded as the main mechanism of heart failure, but pericardiectomy has not always been helpful. Autopsy findings suggest that myocardial fibrosis may play a role in these cases (Tuuteri *et al.*, 1974).

Lipsanen-Nyman et al. (2003) have recently described a 25- year follow-up of 49 MUL patients. They found the pericardium and epicardium to be thickened and fibrotic in 21 of 23 patients undergoing surgery or autopsy. Myocardial cells were hypertrophied with varying fiber diameter and occasional large multiform nuclei. Variable but mostly mild myocardial fibrosis was seen in 7 of 11 autopsied patients.

In the same study (Lipsanen-Nyman *et al.*, 2003), echocardiography was performed on 34 MUL patients (unoperated, n=21) and (operated, n=13) and on 16 healthy controls. According to echocardiographic data, LV hypertrophy but normal systolic function relative to control subjects was found in MUL patients. LV filling was impaired, as suggested by prolongation of late diastolic pulmonary venous flow reversal and an increase in LA size. Echocardiographic measurements did not significantly differ between patients with and without past pericardiectomy.

The study (Lipsanen-Nyman *et al.*, 2003) indicated that although pericardial constriction is the underlying mechanism, myocardial involvement is an important element of MUL cardiopathy and may compromise the results of pericardiectomy.

5.3.4. Left ventricular adaptation to endurance training

LV end-diastolic volume and mass increase after endurance training in healthy individuals (Ehsani *et al.*, 1991, Milliken *et al.*, 1988, Nixon *et al.*, 1991, Scharhag *et al.*, 2002, Wernstedt *et al.*, 2002 , Pluim *et al.*, 2000). LV wall thickness increases, and key features in the distinction between physiological LV hypertrophy and hypertrophic cardiomyopathy are the increased size of LV internal dimensions in endurance-trained subjects, together with normal systolic and diastolic ventricular function.

Previous echocardiographic cross-sectional (Matsuda *et al.*, 1983, Levine *et al.*, 1991, Takemoto *et al.*, 1992, Gledhill *et al.*, 1994) and follow-up (Levy *et al.*, 1993, Shaphiro and Smith, 1983) training studies have shown that LV diastolic function is enhanced with increased fitness. In addition, the LV diastolic dysfunction associated with normal ageing is less pronounced in endurance-trained persons (Levy *et al.*, 1993, Takemoto *et al.*, 1992). Several studies have shown that endurance training increases diastolic filling rate at rest (Levy *et al.*, 1993, Gledhill *et al.*, 1994, Libonati *et al.*, 1999) and during exercise (Nixon *et al.*, 1991, Levy *et al.*, 1993, Gledhill *et al.*, 1994).

The effect of endurance training on the RV has not been widely examined. Endurance athletes tend to have an increased RV thickness and chamber size, which suggests that the RV adapts to endurance training in an analogous manner to the LV (Owen, 2004, Henriksen *et al.*, 1999).

5.3.5. Magnetic resonance imaging techniques for assessment of diastolic function

Cine MRI can be used for evaluation of global ventricular mass, atrial and ventricular volumes, regional wall motion and generation of time-volume curves to assess filling dynamics. It is possible to demonstrate the true distribution of hypertrophy with equal confidence for the anterior and inferior walls, as well as for the apex and RV myocardium (Sipola *et al.*, 2003a). Standard GRE and true FISP techniques are suitable for functional studies, time-volume curves of all cardiac chambers can be determined from cine images. Visualization of turbulent flow in LV outflow tract (Friedrich, 2000, Paelinck *et al.*, 2002) and the valve regurgitations can be seen as a signal void within the bright blood (Sondergaard *et al.*, 1999).

Phase contrast cine MRI can be used to image blood flow dynamics, which reflects global ventricular diastolic function. Changes in the early-to-late filling ratio can be assessed from time-

velocity curves. This technique allows creation of images in which signal intensity is proportional to velocity (Garcia *et al.*, 1998).

Heterogeneity in regional diastolic function can be assessed with myocardial tagging (Kramer *et al.*, 1994, Friedrich, 2000, Paelinck *et al.*, 2002, Lorenz *et al.*, 2000, Earls *et al.*, 2002). Tagging MRI enables the myocardium to be labelled precisely and repeatability between tagging studies is excellent (Paelinck *et al.*, 2002, Reichek, 1999). Tagging MRI is in many ways comparable with tissue Doppler echocardiography (Palka *et al.*, 1999, Garcia *et al.*, 1998). Tissue Doppler also represents the component of motion of a given segment in a direction parallel to the imaging cursor. It can precisely quantify regional LV relaxation and is less sensitive to preload changes (Garcia *et al.*, 1998). Temporal resolution of Doppler echocardiography is very high, in the range of several milliseconds (Hatle and Sutherland, 2000), being superior to that of conventional tagging MRI. However, with the new fast imaging techniques, the images can be obtained every 20 ms yielding a high temporal resolution (Masood *et al.*, 2000, Paelinck *et al.*, 2002).

Diagnostic intracardial findings are similar in restrictive cardiomyopathy and constrictive pericarditis. MRI can be used to discriminate between these two entities. Concurrent pericardial thickening found on MRI confirms the diagnosis of constrictive pericarditis, although the presence of pericardial thickening by itself does not indicate constriction (Frank and Globits, 1999). The pericardium is composed of fibrous tissue and appears dark on T1-and T2 weighted images (Stark *et al.*, 1984). SE images provide the highest anatomical resolution and allow for accurate measurement of pericardial thickness (Soulen, 1991). A non-haemorrhagic, transudative effusion has longer T1 and T2 relaxation times and tend to look dark on T1-weighted spin-echo images and bright on T2- weighted SE or GRE images. Because of higher protein content exudative effusions have greater signal intensity on T1-weighted images, and both the pericardium and pericardial

adhesions may have greater signal intensities than the normal pericardium on T1-weighted images. Haemorrhagic pericardial effusion usually contains areas of both medium and high signal intensity in T1-weighted images, reflecting the variable age of the blood (Frank and Globits, 1999, Axel, 2004). MRI is less sensitive than computed tomography for detecting pericardial calcifications, but larger areas of calcification can be seen as irregularly thickened low-signal areas. In tagged MRI, adhesions between the pericardium and epicardium can be seen by distortion of the tag lines. These adhesive areas are not necessarily associated with areas of the thickened pericardium (Kojima *et al.*, 1999, Axel, 2004).

6. AIMS OF THE STUDY

The general purpose of this work was to evaluate the capacity of MRI for assessing cardiac function, particularly diastolic function.

Specific aims of this study were as follows:

1) To assess characteristic features of MUL cardiopathy and differential diagnosis of constrictive and restrictive cardiomyopathies with MRI. In addition to conventional analysis of LV mass and volume changes during the cardiac cycle, we analysed the pericardium and the function of the RV and both atria (I, II).

2) To assess the effect of endurance training on the early diastolic global and regional LV relaxation and systolic functions with three MRI methods: mitral flow velocity mapping, myocardial four-chamber tagging, and cine MRI (III).

3) To describe a movement correction algorythm and an automated 3-D segmentation method for all four cardiac chambers by combining information on standard short-axis and four-chamber cardiac MR images (IV).

7. METHODS

7.1. SUBJECTS

7.1.1. Assessment of Mulibrey nanism cardiopathy with magnetic resonance imaging (I, II)

MUL is an autosomal recessive disorder that is enriched in the Finnish population. Variable degrees of pericardial and myocardial involvement can lead to heart failure and premature death (Perheentupa, 1973). In Studies I and II, we had the same patient population, except for the one additional male pericardiectomized MUL patient included in Study II. The study population comprised 31 patients (mean age 27 years, range 15-50 years, 17 males, 14 females) with a clinical diagnosis of MUL.

All MUL patients were genetically confirmed with DNA tests. By DNA analysis, all patients were homozycous or compound heterozycous for the Finnish mutations of the TRIM37 gene (Lipsanen-Nyman *et al.*, 2003). We studied two groups of MUL patients. Ten of the 31 MUL patients had undergone pericardiectomy (0.5 – 25 years before our MR study) for constrictive pericarditis. Pericardiectomy was done when the patient had markedly limiting symptoms of congestive heart failure associated with elevated cardiac filling pressures at catheterization. In the surgical treatment, the parietal leaf of the pericardium had been removed from the anterolateral and diaphragmatic aspects of the LV. The removed pericardium was thickened and consisted of scar-like fibrosis devoid of cellularity. Twenty-one MUL patients did not, however, have severe clinical symptoms of congestive heart failure, and had thus not undergone surgery. In Study I, we compared LV results with LV parameters assessed in a normal population matched for gender and height (Marcus *et al.*, 1999), and LA results to normal values reported in the study by Järvinen *et.al*. (1994a).

In Study II, 16 healthy subjects (mean age 31 years, range 19-45 years, 8 males, 8 females) were examined as controls. As patients in Study II had a small body size, we selected control subjects to match this small size better than the values in normal population reported earlier (Marcus *et al.*, 1999, Alfakih *et al.*, 2003b). Body height averaged 1.47±0.10 m vs. 1.54±0.06 m, weight 41.4±8.1 kg vs. 55.4±11.1 kg, and body surface area 1.2 8± 0.16 m^2 vs. 1.51±0.15 m^2 in the MUL and control groups, respectively ($p<0.05$). All patients and controls had sinus rhythm during imaging.

7.1.2. Assessment of the effect of endurance training on left ventricular function (III)

In Study III, 14 healthy sedentary subjects (mean age 43 years, range 23-58 years, 4 males) were examined with MRI before and immediately after (range 3-5 days) a three-month endurance training period. Two subjects were excluded from the study, because they had only undergone one MRI. None of the subjects was taking any medication known to influence cardiac function.

The maximal heart rate of each subject was measured during a maximal bicycle exercise test, and this measurement was used to determine the exercise level for each subject. The subjects exercised at home for three months using a bicycle ergometer. Exercise started at 60% of maximal heart rate for 30 min a day three times a week, and training intensity was gradually increased to 75% of maximal heart rate for 30 min a day four times a week. Subjects used continuous heart rate display (Polar Electro Inc., Finland) to adjust the workload and reported their mean heart rates and exercise duration after each training session.

Exercise tests were done before and after the study period. After training, a bicycle exercise test times improved by 58±53 s (p=0.003) and the increase in peak watts was 9±6% (p=0.002) (Perhonen et al., unpublished data).

7.1.3. Three-dimensional segmentation model for the heart (IV)

In Study IV, cine MRIs of 25 healthy subjects were used as the database (9 healthy controls from Studies I and II, and 16 subjects from Study III, including the two subjects who had undergone only one MRI).

The Human Research Committee of Helsinki University Central Hospital approved Studies I-VI, and all subjects gave their informed consent prior to participation.

7.2. MAGNETIC RESONANCE IMAGING PROTOCOLS

7.2.1. Assessment of Mulibrey nanism cardiopathy with magnetic resonance imaging (I, II)

MRI of the heart was performed with a 1.5T Siemens Vision MR imager and a body array coil. Nine turbo SE T1-weighted images were obtained for the assessment of pericardial thickness. Three images with a 7 mm slice thickness and a 5 mm gap were acquired in the sagittal, axial and coronal planes. Acquisition parameters were TR of one or two RR intervals (mean = 1300 ms), TE = 30 ms, FA = 180^{o}, matrix=256x256, and field of view = 280 - 350 mm.

Breath-hold GRE turbo fast low angle shot cine images in the LV short-axis planes with 10-mm-thick slices and a 5 mm gap were obtained for the volumetric study of ventricles (Alfakih *et al.*,

2004a, Marcus *et al.*, 1999). Cine images in the four-chamber planes with contiguous 10-mm-thick slices were obtained for atria (Järvinen *et al.*, 1994a, Järvinen *et al.*, 1994b). Imaging parameters were TR = 30 or 40 ms, TE = 4.8 ms, FA = 20^{o}, matrix = 256x256, field of view = 250–300 mm.

7.2.2. Assessment of the effect of endurance training on left ventricular function (III)

All subjects were imaged with a 1.5 T Siemens Sonata MR imager (Erlangen, Germany) and a body array coil in supine position. The same MRI protocol was used in studies before and after the endurance training period, and studies were conducted by the same radiologist. All tagged and cine MR sequences were performed during prospective ECG triggering and a breath-hold. MR flow velocity mapping across the mitral valve was performed during free breathing. All subjects had sinus rhythm during imaging.

The volume flow across the mitral orifice was assessed with MR flow velocity mapping and prospective gating using a 2-D flow-sensitive GRE sequence. Velocity encoding was perpendicular to the imaging plane for the mitral valve (= four-chamber view), and the imaging plane was midway between the end-systolic and end-diastolic four-chamber views (Kroft *et al.*, 2000). Velocity sensitivity was set at 150 cm/s to avoid aliasing. Other acquisition parameters were TR = 22 ms (frame rate = 45/s), TE = 4.8 ms, FA = 15^{o}, matrix = 256 x 256, field of view = 320, section thickness = 7 mm.

Two-chamber cine images were obtained to define the plane from the LV apex to the middle of the mitral valve. The four-chamber view for tagging was set perpendicular to the two-chamber view. The four-chamber cine images were labelled with cross-section tag lines at a 90^{o} angle to the interventricular septum. The distance between tag lines was 15 mm. Acquisition parameters were

TR = 51 ms (frame rate = 20/s), TE= 1.5 ms, FA= 20^{o}, matrix = 256x256, field of view = 320 mm. Both diastolic and systolic tagged cine series were obtained.

The systolic tagged cine series was obtained by labelling the LV muscle with tag lines at 0 ms after QRS complex and following the motion of the tags to the end-systole. End-systole was defined as the image with the smallest LV chamber area. The delay to the beginning of diastole was determined from opening of the mitral valve (mean 388 ms, range 345-448 ms), and to end-diastole from its closure. The diastolic tagging cine series were obtained by labelling the LV muscle after that delay and following the motion of the tags to end-diastole.

LV short-axis true FISP cine series were obtained for the assessment of volumetric data of the LV every 15 mm from the LV base to the apex (slice thickness = 7 mm, gap = 8 mm). Acquisition parameters were TR = 34 ms (frame rate = 29/s), TE = 1.5 ms, FA = 20^{o}, matrix = 256x256, and field of view = 360 mm.

7.2.3. Three-dimensional segmentation model for the heart (IV)

Breath-hold cine MR images were obtained in Studies I-III as described in sections 7.2.1 and 7.2.2. In addition in Study III true FISP cine images in four-chamber planes were obtained for volumetric data of the atria every 10mm (slice thickness = 6 - 7 mm, gap = 3 – 4 mm) (Järvinen *et al.*, 1994a, Järvinen *et al.*, 1994b).

7.3. MAGNETIC RESONANCE IMAGING ANALYSIS

7.3.1. Assessment of Mulibrey nanism cardiopathy with magnetic resonance imaging (I, II)

In Studies I and II, all images were manually traced with an image program from the National Institutes of Health (http://rsb.info.nih.gov/nih-image). Pericardial thickness was measured from turbo SE T1-weighted sagittal, axial and coronal images. LV short-axis images were used to measure end-diastolic volume, end-systolic volume, stroke volume and ejection fraction of both ventricles in Studies I and II. Calculations were done according to the modified Simpson's rule, which takes into account the gap between slices (Alfakih *et al.*, 2003b, Soldo *et al.*, 1994). LV end-diastolic length, width and mass were determined. LV mass was calculated by subtracting the chamber volume from the total LV volume (=chamber + muscle) and using 1.05 g/ml as the density factor for the myocardium (Pluim *et al.*, 1997). LV time-volume curves were reconstructed by determining LV volume change per TR (= 30 or 40 ms) from LV short-axis cine images. The volume change during the first third of diastole, the maximal slope during diastole (= peak filling rate) and the time from end-systole to peak rate of LV filling were determined (Rumberger, 1989).

The largest and smallest volumes of both atria were assessed from four-chamber views. (Järvinen *et al.*, 1994a, Järvinen *et al.*, 1994b) Modified Simpson's rule was used in volume analysis (Soldo *et al.*, 1994). Cyclic volume change (largest volume minus smallest volume) and fractional emptying (cyclic volume divided by largest volume) were also determined. One male patient and one female control were excluded from atrial analysis because of poor image quality.

7.3.2. Assessment of the effect of endurance training on left ventricular function (III)

In Study III, mitral valve inflow was segmented manually with an image program from the National Institutes of Health. The averaged velocity in the ROI was determined and then multiplied by the cross-sectional area of the mitral valve contours to generate a flow volume measurement (mean blood flow = mean velocity * cross-sectional area) (Szolar *et al.*, 1996). The velocity inflow curves were reconstructed. Diastolic function parameters derived from the inflow curves, including the time to peak early filling, the peak early filling rate, the deceleration time of early diastolic wave, the duration of early diastolic wave (Paelinck *et al.*, 2002) and the early filling volume (Pluim *et al.*, 1998) were determined.

The beginning and the end of early diastole were determined from the velocity inflow curve across the mitral valve. Longitudinal tagging analysis was performed manually at midmyocardium, perpendicular to the tag lines. The distance between basal and apical tag lines (= distance between six lines) was measured on the septum and the LV lateral wall at the beginning and the end of early diastole. The early diastolic myocardial relaxation velocities and fractions were determined. Systolic analysis was done similarly from systolic tagging series, and systolic myocardial contraction velocities and shortening fractions were determined. Tagged images of one male were excluded because of gating problems and those of another male because of the failure of mitral valve MR flow velocity mapping before training (total number of subjects=12).

Regional differences in the distance between three apical and three basal tag lines were determined to assess diastolic myocardial relaxation and systolic myocardial contraction in the septum and in the LV lateral wall. Diastolic myocardial relaxation fraction, systolic myocardial shortening fraction, myocardial relaxation and contraction velocities (mm/s) were determined (= change

between lines (mm) / relaxation or contraction time (s)). Tagged image data of one male was excluded because of gating problems (total number of subjects =13).

Assessment of LV volumes was done from LV short-axis images manually. End-diastolic and end-systolic volumes were calculated according to the modified Simpson's rule. The LV mass was determined by subtracting the cavity volume from the total LV volume (= cavity + muscle) and using 1.05 g/ml as the density factor for the myocardium.

7.3.3. Three-dimensional segmentation model for the heart (IV)

The segmentation method consists of two steps: 1) correction of movement artefacts from short-axis and four-chamber images and 2) segmentation of images by non-rigidly matching an a priori model to both image series simultaneously.

Because the short-axis and four-chamber image series were acquired during the same imaging session, the image headers contained all necessary information to compute the location of each voxel relative to the imaging device. However, the movement artefacts, such as breath-hold level reproducibility, are not taken into account if only header information is used to define the voxel-by-voxel correspondences. A novel algorithm was developed to register (align) the short-axis images based on four-chamber images, and vice versa. A similarity measure based on normalized mutual information was maximized between 3-D short-axis and four-chamber view volumes (Lötjönen, 2004b) (Figure 11).

The 3-D shape model was built from the first image of each time series, from the end-diastolic phase. Both short-axis and four-chamber views were used to build the shape model, therefore voxel-by-voxel based correspondence needed to be defined between the image volumes.

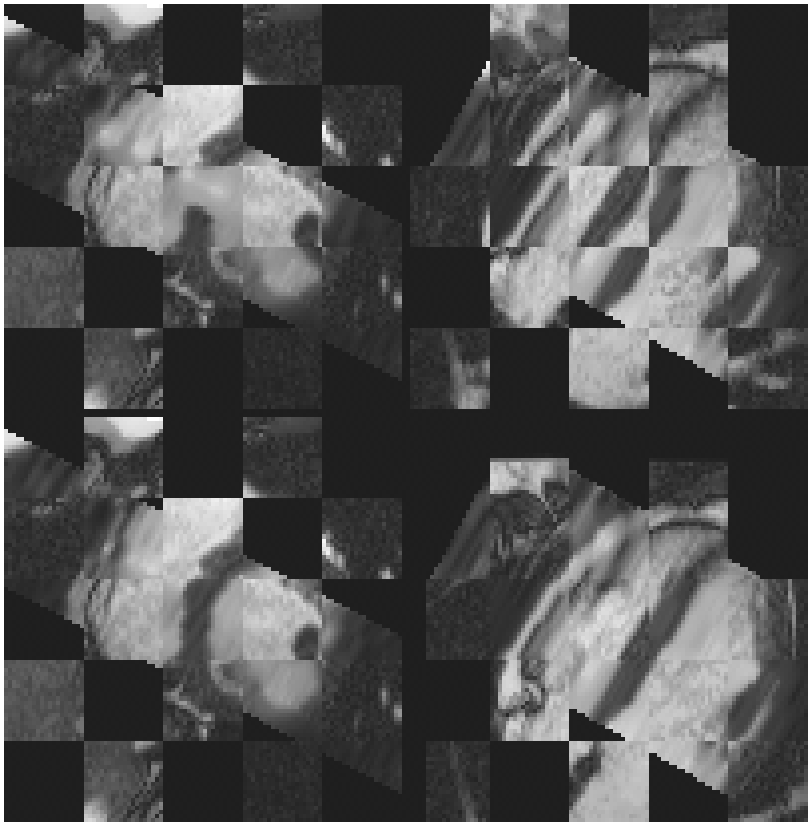

Figure 11. A movement correction algorithm to register the short-axis images based on four-chamber images, and vice versa

The segmentation method was based on deformable models where an a priori model is non-rigidly registered to target data by maximizing similarity between data. The a priori model built in this work represented a mean heart shape of 25 healthy subjects. In addition, the variability of the shape was modelled and utilized to constrain the shape changes in a non-rigid registration. The novelty of the segmentation algorithm is that both short-axis and four-chamber views can be used in assessment of the cavity volumes. The tool showed three cross-sections of the cavity volume, and the deformations could be made in any of these cross-sections. This allows more accurate reconstruction of ventricles and also segmentation of atria.

In the model construction, atria, ventricles and the epicardium were manually segmented from images of all subjects with a software tool designed for interactively making 3-D deformations. (Lötjönen, 2003a) With this tool, a triangulated surface model was registered manually and non-rigidly to edges in the short-axis and four-chamber image volumes. The tool showed three cross-sections of the cavity volume, and the deformations could be made in any of these cross-sections (Figure 12).

The following guidelines were used in manual segmentation. The basal regions of the RV and LV were defined using the four-chamber images. The atrioventricular valves were used as an interface between atria and ventricles, but because the valves move throughout the cycle, the most basal points of the myocardium were defined. The boundaries between both atria and ventricles were approximated by a straight line between the points in each slice. Because segmentation of the apex on short-axis images is inaccurate, it was located on the four-chamber images. The pulmonary artery was not included in the RV in the model. The pulmonary valve level was difficult to locate from basal short-axis slices. A compromise was made, and a smooth boundary was created from the slice where the artery was visible to a more apical slice, which definitely contained only the RV.

The inferior and superior vena cava were excluded from the RA and the pulmonary vein inlets were excluded from the LA. Two LV segmentations were made with and without papillary muscles. The epicardial boundaries were also segmented.

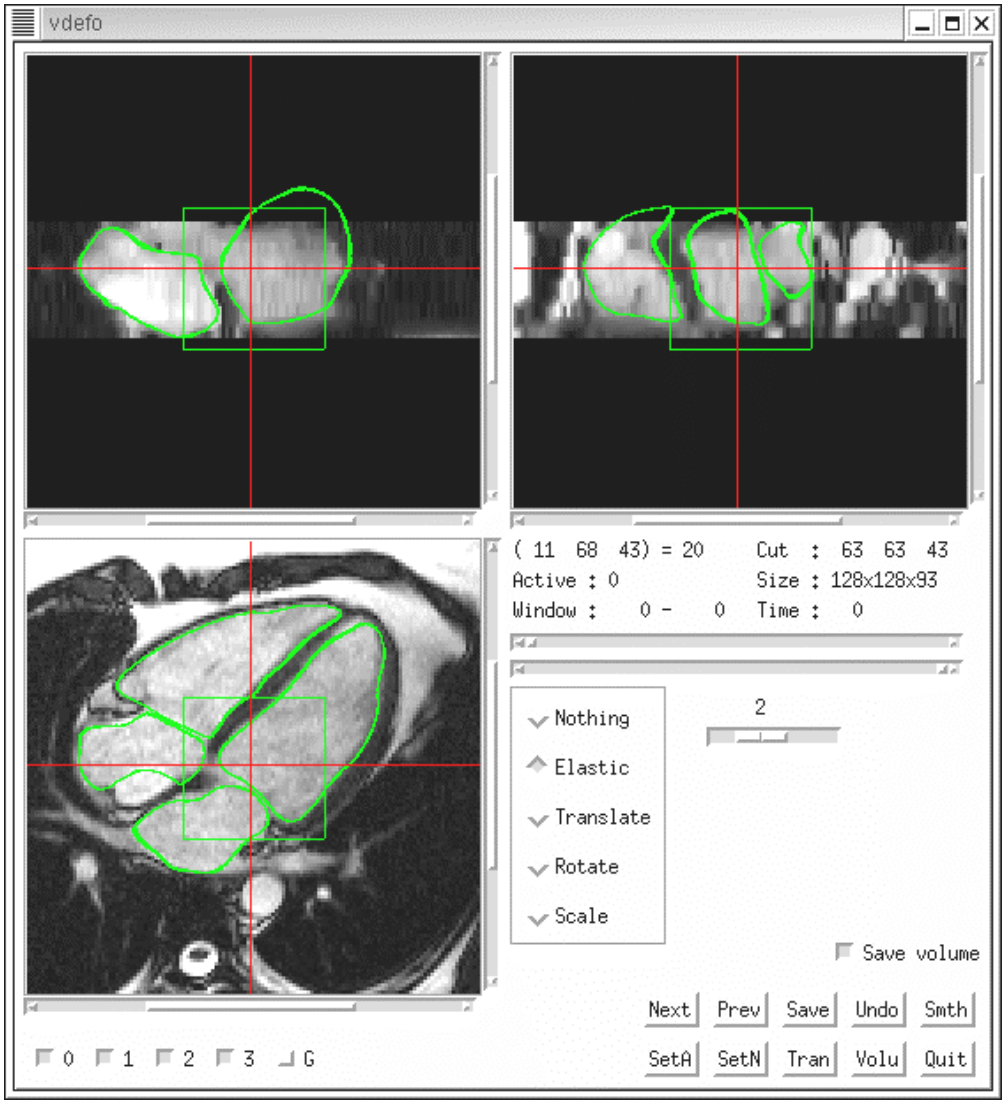

Figure 12. A software tool for manual segmentation

The triangulated model has been superimposed on MR data. The accuracy and coherency of manual segmentation is very important for the accuracy of volumetric measures as well as for the functionality of the automated tool because all inaccuracies in the model will be directly transformed to the final result of the automated tool.

7.4. STATISTICAL ANALYSIS

In Study I, MUL patients were divided into groups with (n=9) and without (n=21) a history of pericardiectomy. LV volume and function results were compared with individually normalized values of LV in relation to gender and height (Marcus *et al.*, 1999). LA parameters were normalized to body surface area and LV stroke volume to compare them with reference values (Järvinen *et. al.* 1994a). Student's t-test was used to detect significant differences. A p-value of <0.05 was considered to indicate statistical significance.

In Study II, MUL patients were divided into groups with (n=10) and without (n=21) a history of pericardiectomy. They were compared with each other and with normal controls (n=16). Comparisons across the three group means were done using analysis of variance (ANOVA) incorporating sex as a second grouping factor. To adjust for differences in body size, body height and weight were used as covariates when comparing MRI data on cardiac anatomy between the MUL patients and the controls. A p-value of <0.05 was considered to indicate statistical significance. All statistical analyses were performed with commercially available software (SYSTAT version 10.1, Systat Inc.).

In Study III, non-parametric tests were used, since the study group was small. The Wilcoxon signed-rank test was used to compare the results before and after the training period, and Spearman's two-tailed correlation coefficient to determine correlations. A p-value of <0.05 was considered to indicate statistical significance. All statistical analyses were performed with commercially available software (SPSS version 11.1.01)

In Studies I-III, intraobserver variability was calculated with the Bland and Altman (1986) method, which plots the difference between the two results against their average. In Studies I and II, the mean difference and standard deviation of the LV mass and the LA and LV volumes were calculated. In Study III, intraobserver variability in tagging analysis was measured. A p-value of <0.05 was considered to indicate statistical significance. In addition, correspondence between the beginning and the length of early diastole in the mitral velocity inflow curve and in four-chamber myocardial tagging was analysed.

In Study IV, we compared manual segmentation results of both ventricles measured from short-axis images and from a triangulated combination of short-axis and four-chamber images. The mean difference in ventricular volumes was obtained by subtracting the size of ventricles measured from short-axis images from the size of ventricles measured with a triangulated combination, and the mean of differences was tested with the Bland and Altman (1986) method. In comparison between a triangulated manual and automated segmentation model, segmentation error was defined as mean distance from the surface of the automatic shape model to the surface of the corresponding manually segmented surface. Manual segmentation was considered the reference method (= gold standard). A non-parametric Wilcoxon signed-rank test was used to detect statistically significant differences between manual segmentation measured from short-axis and four-chamber images, and to compare manual and shape model segmentation results. A p-value of <0.05 was considered to indicate statistical significance.

8. RESULTS

8.1. Assessment of Mulibrey nanism cardiopathy with magnetic resonance imaging (I, II)

Heart rate was similar in both groups (MUL 70+11/min, controls 67+16/min, p= 0.29). Significant valvular failures were not observed (Lipton and Coulden, 1999). The thickness of the pericardium was normal (< 3.5mm) in all MUL patients (Stark *et al.*, 1984, Hartnell *et al.*, 1996). In the ten pericardiectomized patients, the remnants of the pericardium were of normal thickness as well. Pericardial fluid was not present. The maximal thickness of the parietal pericardium was 3.3 mm around the RV posterior wall in one patient, and less than 2.9 mm in the rest.

In Study I, the largest and smallest LA volumes, LV volumes and cardiac outputs were lower in MUL patients than in normal healthy adults. LV systolic function was mainly preserved in MUL patients, but diastolic 1/3 filling was rapid in LV time-volume curves. LA cyclic volume change was also reduced compared with values of normal subjects (13$\pm$4 ml vs. 20$\pm$2 ml).

In Study II, we found, that LV and RV end-diastolic volumes adjusted for body height and weight were significantly smaller in MUL patients than in controls. In MUL patients, the interventricular septum ($p<0.001$) and the LV posterior wall ($p<0.001$) were thicker, but the LV mass was not significantly higher than in controls.

The end-diastolic length/width ratio of LV was significantly smaller in patients than in controls (MUL 1.55$\pm$0.2, controls 1.73$\pm$0.3, $p<0.05$). The LV ejection fraction did not differ between the two groups, but the RV ejection fraction was lower in MUL patients (Table 1).

Sex had an independent effect on thickness of the LV posterior wall (male 10.0±0.5 mm, female 12.0±0.5 mm, p=0.025) and the LV ejection fraction (male 67±2%, female 57±2%, p<0.001). There were no statistical differences between patient groups with and without pericardiectomy. MUL patients had a larger early 1/3 diastolic volume change, a reduced absolute peak filling rate and a shorter time to the point of peak rate of LV filling (Table 2).

The atrium to ventricle ratio of both right and left sides in MUL patients was increased, indicating mild dilatation of both atria. Cyclic volume change and fractional emptying of both atria were lower in MUL patients, especially in those who had not had a pericardiectomy (Table 3).

Significant differences were not found between MUL patient groups with and without pericardiectomy in Studies I and II. Intraobserver variability for manual segmentation studies (n=12) expressed as bias±1 standard deviation of the difference in LV EDV 1± 6 ml (p>0.05), LA maximal volume 1± 3 ml (p>0.05), and LV mass 2±9 g (p>0.05) (Kivistö *et al.,* unpublished data).

Table 1. Ventricular volumes LV mass and wall thickness of 31 Mulibrey nanism (MUL) patients and 16 healthy controls

	MUL patients (n=10) pericardiectomy +	MUL patients (n=21) pericardiectomy -	Controls (n=16)	P-value
LV end-diastolic volume (ml)	75±5	76±8	104±6	0.008
LV mass (g)	107±6	105±9	85±7	0.104
Interventricular septal thickness (mm)	9.0±0.4	10.4±0.6	6.6±0.5	0.001
Posterior wall thickness (mm)	12.6±0.4	11.2±0.6	9.3±0.5	<0.001
LV ejection fraction (%)*	63±2	61±3	62±2	0.755
RV end-diastolic volume (ml)	51±5	57±8	98±6	0.000
RV ejection fraction (%)*	51±2	47±3	62±2	<0.001

Values are mean ± standard deviation. Adjusted for body height and weight.
LV=left ventricle, RV=right ventricle.
P-values across the three groups from ANOVA, with sex as a second group factor and height and weight as covariates.
* group comparisons made without adjusting for differences in body size.

Table 2. Diastolic filling variables assessed by left ventricular diastolic time-volume curve in Mulibrey nanism (MUL) patients and controls

	MUL patients (n=31)	Controls (n=16)	P-value
Volume change during the first third of diastole (%)	72±2	63±3	0.030
PFR (ml/s)	311±23	393±33	0.047
TPF (s)	96±9	131±13	0.030

Values are mean ± standard deviation.

PFR = absolute peak filling rate, TPF = time from end-systole to occurrence of peak rate of ventricular diastolic filling. P-values across the three groups from ANOVA, with sex as a second group factor. Sex had no significant main effect on or interactions with any variable.

Table 3. Atrial volumes of 30 Mulibrey nanism (MUL) patients and 15 healthy controls

	MUL patients (n=10) pericardiectomy +	MUL patients (n=20) pericardiectomy -	Controls (n=15)	P-value
LA largest volume (ml)	49±4	45±6	48±5	0.860
LA smallest volume (ml)	34±2	33±4	28±3	0.321
RA largest volume (ml)	50±4	48±6	49±5	0.972
RA smallest volume (ml)	35±3	35±5	30±4	0.618
Left atrium/ventricle ratio	0.63±0.04	0.64±0.06	0.50+0.04	0.062
Right atrium/ventricle ratio	0.64±0.04	0.67±0.06	0.53±0.05	0.093
LA cyclic volume (ml)	14±1	13±2	20±2	0.048
RA cyclic volume (ml)	13±2	12±2	20±2	0.041
LA fractional emptying (%)	31±2	26±2	40±2	0.009
RA fractional emptying (%)	29±2	25±3	38±2	0.001

Values are mean ± standard deviation. Adjusted for body height and weight.
LA = left atrium, RA = right atrium. P-values across the three groups from ANOVA, with sex as a second group factor and height and weight as covariates. Sex had no significant main effect on or interactions with disease status.

8.2. Assessment of the effect of endurance training on left ventricular function (III)

Training lowered heart rate (before training 73±9/min vs. after training 64±9/min, p=0.009) and systolic blood pressure (118±17 mmHg vs. 112±14 mmHg, p=0.027). Diastolic blood pressure at rest, weight (74.5±15.5 kg vs.73.8±14.5 kg), and body surface area (1.82±0.21 m^2 vs. 1.82±0.2 m^2) did not change. After training, end-diastolic volume did not increase significantly, but end-systolic volume decreased, ejection fraction increased (Kivistö *et al*., unpublished data) and LV mass increased (Table 4).

The time to peak early filling shortened. The peak early filling rate, the deceleration time of early diastolic wave and the duration of early diastole did not decreased significantly. The early filling volume did not change significantly either (Table 5).

After training, the early myocardial relaxation fraction and velocity increased both in the septum and in the LV lateral wall (Table 5). As there were longer TRs in the tagging image sequence than in the MR flow velocity sequence (51 ms vs. 22 ms), the correspondence between the beginning (mean difference 1.2 ms ± standard deviation 14.9) and the duration (1.4 ± 22.7 ms) of early diastole was tested with the Bland and Altman method. The beginning (before training $r = 0.975$, $p < 0.001$; after training $r = 0.924$, $p < 0.001$) and the duration (before training $r = 0.855$, $p < 0.001$, after training $r = 0.778$, $P = 0.730$) of the early diastole in flow velocity curves across the mitral valve and in the tagged early diastolic analysis had a good correlation.

In regional analysis of the septum and LV lateral wall, myocardial relaxation was more pronounced in the basal septum (p=0.02).

According to systolic tagging analysis of the septum and the LV lateral wall, systolic contraction did not change significantly after training (Table 6). However, in regional tagging analysis, myocardial contraction velocity ($p=0.028$) and shortening fraction ($p=0.009$) were more pronounced in the apical septum (Kivistö *et al.,* unpublished data).

The intraobserver variability in tagging analysis (n=30), expressed as bias $\pm$ 1 standard deviation of the difference, was 0.5 ± 2.9 mm ($p>0.05$) (Kivistö *et al.,* unpublished data).

Table 4. The left ventricular volumetric data before and after a three-month endurance training period in healthy subjects (n=14)

Left ventricle	Before training	After training	P-value*
End-diastolic volume (ml)	121±19	125±23	0.233
End-systolic volume (ml)	47±11	42±13	0.030
Ejection fraction (%)	62±5	66±7	0.014
Mass (g)	97±19	105±18	0.005

Values are mean ± standard deviation. *P-value of < 0.05 indicates statistical significance.

.

Table 5. Early diastolic flow velocity measurements and a comparison with left ventricular (LV) early diastolic tagging measurements in healthy subjects (n=13)

	Before training	After training	P-value*
Flow velocity measurements			
Time to peak early filling (ms)	110±30	100±20	0.021
Peak early filling rate (ml/s)	440±130	420±80	0.136
Deceleration time of early diastolic wave (ms)	160±30	150±20	0.227
Duration of early diastole (ms)	270±30	260±30	0.327
Early filling volume (ml)	56±18	55±12	0.239
Early diastolic tagging measurements			
Early septal myocardial relaxation fraction (%)	23±60	26±58	0.056
Early septal myocardial relaxation velocity (mm/s)	70±18	93±29	0.002
Early LV lateral wall myocardial relaxation fraction (%)	22±85	29±38	0.002
Early LV lateral wall myocardial relaxation velocity (mm/s)	69±26	99±21	0.002

Values are mean ± standard deviation. *P-value of < 0.05 indicates statistical significance.

Table 6. Systolic four-chamber tagging results in the septum and the left ventricular (LV) lateral wall before and after a three-month endurance training period in healthy subjects (n=13) (Kivistö *et al*., unpublished data)

	Septum			LV free wall		
	Before training	After training	P-value*	Before training	After training	P-value*
Myocardial shortening fraction (%)	11±4.6	13±0.3	0.046	12±0.6	14±0.4	0.152
Myocardial shortening velocity (mm^{-}/s)	29.2±15.6	35.3±17.8	0.249	31.7±18	38.3±15.6	0.100

Values are mean ± standard deviation.

*P-value of < 0.05 indicates statistical significance.

8.3. Three-dimensional segmentation model for the heart (IV)

The comparison between LV and RV volumes measured manually from short-axis images and triangulated from short-axis and four-chamber images showed that short-axis analysis misses basal and apical volumes of both ventricles. The volumes of LV and RV (n=16) were 6.6 ± 8.9% and 7.1 ± 4.5% smaller when measured only from short-axis images (Lötjönen *et al.,* unpublished data) (Figure 13 a,b, Table 7).

The ventricles dominated in the automated initialization because of larger volume. The automatic segmentation accuracy in the ventricles was therefore notably better than in the atria. In addition segmentation of atria was more difficult as there is no clear boundary between atria and vessel inlets. The mean distance with standard deviation from the deformed surface of the best shape model to the manually segmented surface was in the LV 2.01 ± 0.31 mm, in the RV 2.37 ± 0.05 mm, in the LA 2.56 ± 0.88 mm, in the RA 2.93 ± 1.30 mm and in the epicardium 2.77 ± 0.44 mm. The average of all surfaces was 2.53 ± 0.70 mm. When the data of four subjects were manually segmented twice, the average error of all surfaces was 1.75 mm, and using the shape model for the same subjects 2.57 mm.

Table 7. Comparison between manual segmentation results of both ventricles (n=16) measured from short-axis images only and from a triangulated combination of short-axis and four-chamber images

	Short-axis image segmentation	Triangular segmentation (short-axis +four-chamber)	P-value
Left ventricle ml	131±26	141±27	> 0.001
Right ventricle ml	114±26	123±29	0.013

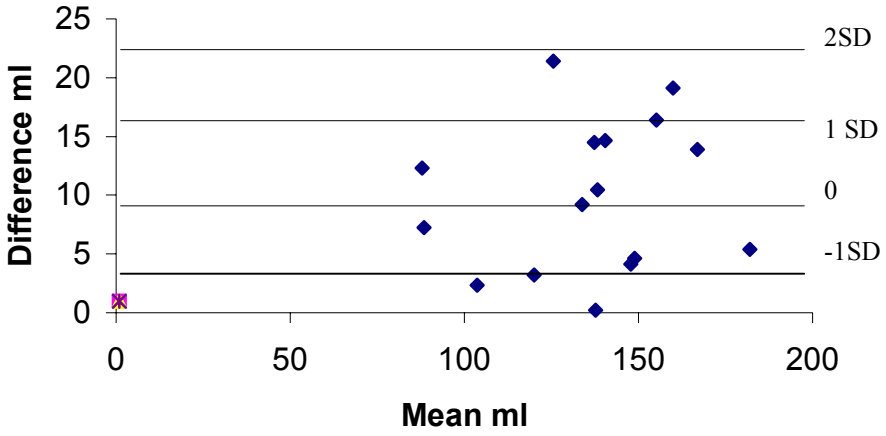

Figure 13 a.

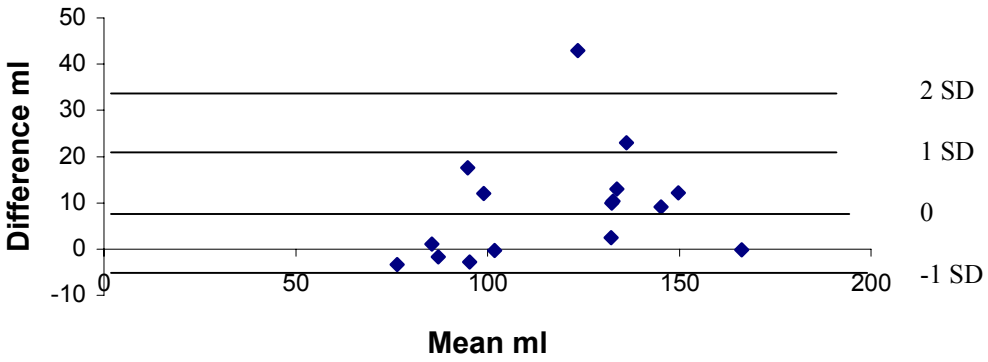

Figure 13 b.

Figure 13 a, b. The mean difference in ventricular volumes was obtained by subtracting the size of ventricles measured short-axis images from the size of ventricles measured from combinated short-axis and four-chamber images, and calculated the mean of differences as suggested by Bland and Altman (1986)

Figure 13 a. Left ventricle: 9.9 ± 6.4 ml, $p<0.05$

Figure 13 b. Right ventricle: 9.1 ± 11.9 ml, $p<0.05$

9. DISCUSSION

9.1. Assessment of Mulibrey nanism cardiopathy with magnetic resonance imaging (I, II)

In assessing MUL cardiopathy with MRI, pericardial thickness was found to be normal in all MUL patients. In the 10 pericardiectomized patients, the remnants of the pericardium were of normal thickness as well. Both ventricular diastolic volumes were decreased, whereas LV wall thickness was increased. The length/width ratio of the LV was significantly smaller in MUL patients. The LV diastolic filling was altered in a restrictive manner, although systolic function was preserved. The RV ejection fraction was reduced. Both atria were mildly enlarged, and the reservoir function of both atria was diminished.

In addition to earlier echocardiographic findings by Lipsanen-Nyman *et al*. (2003), we discovered the following features of MUL cardiopathy: 1) The thickness of the pericardium was normal in the patient group (n=21) that had not needed pericardiectomy for congestive heart disease. 2) The shape of the LV cavity was different in MUL patients, with a smaller end-diastolic length/width ratio, as compared with normal controls. With MRI, we acquired more accurate results for LV mass and cyclic volumes than echocardiography, which uses an ellipsoidal model for measurements (Pluim *et al.*, 1997). 3) The RV diastolic volumes were lower than in controls. 4) Volumetric data of both atria showed relative dilatation compared with the ventricles, as well as decreased reservoir function. Both of these findings are indicative of ventricular restriction in MUL cardiopathy.

The thickness of the pericardium was normal in the patient group (n=21) that had not needed pericardiectomy for congestive heart disease. Turbo SE T1-weighted images were used to assess pericardial thickness, allowing a precise determination of the thickness (Masui *et al.*, 1992).

The end-diastolic volumes of both ventricles were decreased compared with controls in patients with or without pericardiectomy. Earlier studies have found that LV volumes are normal or decreased in patients with diastolic heart failure (Zile *et al.*, 2004, Kitzman *et al.*, 2002, Tsutsui, 2001, Warner *et al.*, 1999). Although LV systolic function was preserved, the RV ejection fraction was reduced, suggesting elevated afterload due to LV diastolic impairment. In MUL cardiopathy, myocardial fibrosis and hypertrophy combined with an adhered visceral pericardium, result in reduced diastolic ventricular volumes, even in patients with previous pericardiectomy. The volume change during the first third of LV diastole was larger, the absolute peak filling rate was reduced and the time to peak filling was significantly shorter in MUL patients than in controls, and no difference was present in these measurements between patients with and without past pericardiectomy. Taken together with the reduced LV end-diastolic volume, these changes suggest an increased speed of early LV filling due to impaired passive filling during later diastole. LV filling is altered in a restrictive manner, and is due to both myocardial and pericardial abnormalities.

A difference was present in the shape of the LV chamber in MUL patients, with a smaller end-diastolic length/width ratio, as compared with normal controls. MR cine imaging is the method of choice in the volumetric assessment of both left and right sides of the heart (Soldo *et al.*, 1994, Järvinen *et al.*, 1994a, Järvinen *et al.*, 1994b, Pattynama *et al.*, 1995). More accurate results for LV mass and cyclic volumes were thus acquired than with echocardiography, which uses ellipsoidal model for measurements (Pluim *et al.*, 1997). In MUL patients, the muscle of the interventricular

septum and the posterior wall were thicker than in controls. Because of the shorter LV, the LV mass was increased, but not significantly.

A limitation in Study I was that normal LA and LV values reported in normal subjects (Järvinen *et al.*, 1994a) or normalized in a normal population (Marcus *et al.*, 1999) are not necessarily comparable with values in small-sized adult MUL patients. In study II, MUL patients and control groups were also not fully matched for body size. Moreover, the same patients were not studied before and after pericardiectomy.

The intraobserver variability in the assessment of LA and LV volumes and LV mass was low and parallel to early studies (Alfakih *et al.*, 2003b, Myerson *et al.*, 2002). As described earlier, the MRI is very accurate and reproducible method to study cardiac volumetry and LV mass. Therefore the numbers of subjects needed for similar studies with cardiac MR are as few as 1/10 of that requires using echocardiocraphy.(Myerson *et al.*, 2002, Pattynama *et al.*, 1995)

9.2. Assessment of the effect of endurance training on left ventricular function (III)

After training, LV mass increased indicating physiological LV hypertrophy. In addition LV ejection fraction increased. The time to peak early filling shortened. Early diastolic myocardial relaxation in the septum and LV lateral wall increased. In regional tagging analysis myocardial relaxation was pronounced in the basal septum and contraction in the apical septum.

The end-diastolic volume did not change after three months of training, but LV mass and ejection fraction at rest increased significantly. In previous echocardiography and MRI studies (Scharhag *et al.*, 2002, Pluim *et al.*, 1998, Wernstedt *et al.*, 2002, Nixon *et al.*, 1991, Milliken *et al.*, 1988,

Ehsani *et al.*, 1991, Fagard, 2003, Finkelhor *et al.*, 1986), LV end-diastolic volume and mass have increased, and ejection fraction at rest has remained unaltered after endurance training.

In mitral flow velocity mapping, the time to peak early filling shortened after training, indicating an improvement in global LV early myocardial relaxation. This result is in concordance with earlier echocardiography studies (Dubach *et al.*, 1997, Levy *et al.*, 1993, Matsuda *et al.*, 1983, Myers *et al.*, 2002, Nixon *et al.*, 1991).

Early diastolic longitudinal myocardial relaxation in the septum and LV lateral wall increased in the four-chamber tagging, which indicates pronounced early diastolic regional myocardial relaxation after training. In regional tagging analysis, we also found regional differences; diastolic myocardial relaxation was more pronounced in the basal septum, and myocardial contraction in the apical septum. Few previous longitudinal echocardiographic studies comparing results before and after a supervised training period in normal subjects have been published (Shaphiro and Smith, 1983, Levy *et al.*, 1993). No earlier follow-up MRI studies of the effect of endurance training on LV regional function in normal subjects, as assessed by myocardial tagging exist. Myers *et al.* (2002) studied the effects of endurance training on LV diastolic and systolic function with tagged MRI in non-ischaemic cardiomyopathy patients. They observed that the LV diastolic rotational relaxation velocity increased significantly after a two-month endurance training period, but systolic function did not change. Bogart and Rademakers (2001) found regional functional non-uniformity in normal LV, and Myers *et al*. (2002) reported the effect of training to be more pronounced in diastolic than in systolic regional function.

Retrospective EKG-gated sequences were not available at the time of imaging of the subjects, and thus, we used prospective gating. Late diastolic information of atrial contraction was therefore

missed, and we concentrated on early diastolic results. Although four-chamber tagging analysis determines only longitudinal movement, it is in the context of rotational movement. Accurate determination of functional changes requires a temporal resolution of < 40 ms (frame rate > 25/s) (Fujita *et al.*, 1993, Hartiala *et al.*, 1993). Temporal resolution of our cine and flow sequences was 34 ms (frame rate 29/s) and 22 ms (frame rate 45/s), respectively. In the tagging sequence, TR was 51 ms (frame rate 20/s) lower than recommended; we therefore determined the beginning and the end of early diastole from mitral velocity inflow curves. Modern acquisition techniques allow a high temporal resolution of ≤ 20 ms in cine, flow and tagging sequences (Kuhl *et al.*, 2004, Paelinck *et al.*, 2002).

We assessed LV function with cine MRI, mitral flow velocity mapping and MRI myocardial four-chamber tagging. With cine MRI, it is possible to determine end-diastolic and systolic volumes and to reconstruct time-volume curves. Mitral flow velocity mapping enables determination of ventricular flow and reconstruction of time-velocity curves. These two methods determine ventricular global function. Several physiological variables simultaneously affect to flow velocities and may have confounding effects on ventricular inflow (Ommen *et al.*, 2000). The MRI myocardial four-chamber tagging method assesses regional myocardial function, and similarly to tissue Doppler, it is less sensitive to preload changes (Garcia *et al.*, 1998). The major advantage of myocardial tagging method is high reproducibly, and also in our study intraobserver variability was low ($p>0.05$). The increase in distance between tag lines is related to longitudinal diastolic myocardial relaxation and diastolic filling (Mandinov *et al.*, 2000).

9.3. Three-dimensional segmentation model for the heart (IV)

Study IV presents a movement correction algorithm and a new technique to reconstruct cardiac 3-D geometry from multiple images. Our segmentation results are, however, preliminary and done with a small study population. Manual segmentation of ventricles from short-axis data underestimates total ventricular volumes by about 7%, as it omits the basal and apical parts of the ventricles. With the segmentation method, borderlines between atria and ventricles can be more accurately determined. Intraobserver variability between the triangulated manual segmentation and the automatic segmentation was essentially similar as described earlier (Lorenzo-Valdes´ *et al.*, 2004, Mitchell *et al.*, 2002). Our segmentation technique utilizes both short-axis and four-chamber images. In previous automated segmentation studies, only short-axis images have been used to define the volumetry of LV (van der Geest *et al.*, 2004, Mitchell *et al.*, 2002, Graves *et al.*, 2000) and recently also RV (Lorenzo-Valdes´ *et al.*, 2004).

In addition to both ventricles, a shape model of the atria was built. As we know, segmentation methods for the atria have not been performed earlier in an automated framework. This new approach, which combines information from standard short-axis and four-chamber images, facilitates modelling of the atria as well as the basal and apical regions of the ventricles. The data for segmentation were acquired using a standard protocol for cardiac patients. A smaller slice separation would have yielded a better spatial resolution, and the short-axis images would have also contained atria resulted in more comprehensive information. Although data sets were not optimal for the model construction, the advantage in using standard sets is that no specific imaging protocols are needed to increase the size of the database.

Missregistration of slices in 3-D segmentation was corrected with our movement correction algorithm. A good indication of successful movement correction was that the edges both in atria and ventricles became more continuous. Movement correction algorithms are valuable in 3-D segmentation so long as the very resent technical advances, which make possible to image volymetric datasets covering the heart in the single breath-hold became more common (Kozerke *et al.*, 2004).

Segmentation is one of the most difficult aspects of image processing. The difficulty arises from noise in images, image inhomogeneities, partial volume effect, complex and cluttered scenes and low visibility of edges between objects. Deformable model-based methods provide one approach to partially overcome the problem. In these methods, an a priori model is non-rigidly registered to the object of interest in the image by optimising a cost function.

Statistical modelling of different populations will be a field of increasing importance in the future, as automated methods will facilitate the modelling of variability between humans on a large scale. Importantly, some information can not be differentiated visually from images, when only small differences exist between healthy and pathologial populations (Sievers *et al.*, 2004). Before applying the shape model to population studies, several issues related to various error sources need to be considered. In the future, the 3-D statistic shape model is anticipated to be extended to a dynamic 4-D model, enabling determination of volume changes in all four cardiac chambers throughout the cycle (Lorenzo-Valdes´ *et al.*, 2004).

10. CONCLUSIONS

MRI is a reliable method to assess cardiac anatomy, systolic and diastolic function. Diastolic global and regional function can be determined with different MRI methods; flow-velocity mapping, myocardial tagging and cine MRI.

1) Based on MRI, MUL cardiopathy was characterized by concentric LV hypertrophy and restrictive filling due to both myocardial and pericardial abnormalities. Although LV systolic function was preserved, both atria were mildly enlarged and cyclic volume change of both atria were reduced. In addition RV ejection fraction was reduced. All these features suggested an elevated afterload due to LV diastolic impairment.

2) Physiological LV hypertrophy was found after a three-month endurance training period in healthy subjects. According to mitral flow velocity mapping and four-camber tagging global and regional LV, early diastolic relaxation improved. Regional early diastolic myocardial relaxation improved significantly both in the septum and in the lateral wall. Myocardial relaxation was more pronounced in the basal septum, and contraction in the apical septum. Four-chamber tagging is a valuable clinical tool with excellent reproducibility for determination of regional differences in myocardial regional diastolic and systolic movements.

3) Misregistration of slices was possible to correct using our movement correction algorithm, and the edges both in atria and ventricles became more continuous. A new automated 3-D segmentation method for all four cardiac chambers was developed by combining information on standard short-axis and four-chamber cardiac MR images. In the future, 4-D segmentation will likely permit accurate determination of time-volume curves of all four cardiac chambers.

11. ACKNOWLEDGEMENTS

This thesis is based on work carried out during 1999-2005 at Helsinki Medical Imaging Center, Helsinki University Central Hospital.

My deep appreciation is due to CEO, Docent Juhani Ahovuo for providing exellent research facilities at the Helsinki Medical Imaging Center. I am also sincerely grateful to Professor Leena Kivisaari of the University of Helsinki, for her encouraging support throughout project.

I owe a large dept of thanks to my supervisors Docent Kirsi Lauerma and Docent Pauli Hekali for their continuous support and guidance. I met Kirsi for the first time in 1999, when my study project began. Since then she has helped me in innumerable ways and taught me nearly everything I know about cardiac MRI and study work.

I warmly thank all of co-authors. Special thanks are due to Marita Lipsanen-Nyman and Docent Markku Kupari for generous help and support in the Mulibrey nanism project. My deepest gratitude is also due to Docent Jyrki Lötjönen, who has been very helpful and patient with me concerning image segmentation and writing of this thesis. I also thank Merja Perhonen, who has been most helpful each time I have contaced her and has encouraged me to go on with the difficult tagging analysis.I also thank Juha Koikkalainen and Daniel Smutec for co-authorship.

A very special thank-you goes to colleague and close friend Miia Holmström, who has been my side both studies and family projects. I am so grateful for her help in good and bad times.

During the course of this study I have been fortunate to get to know Docent Taina Autti, who is a great scientist and humanitarian. She has helped and encouraged me in so many ways in this work. She also has a wonderful sense of humour, and we have laughed together countless times. Never give up, Taina!

My warmest appreciation goes to the official reviewers, Docent Johanna Kuusisto from the University of Kuopio and Professor Jaakko Hartiala from the University of Turku, for constructive and valuable comments on the manuscript. I warmly thank Carol Ann Pelli for editing of the language.

I am lucky to have many good friends and colleagues which I want to warmly thank: Merja Raade, Ulla Kotilainen, Sami Soljanlahti, Anna Maria Pie`, Maria Krause, Leif Holmberg, Tuula Seppänen, Helena Hänninen, Maria Sippola-Soininen, Liisa Pekkanen, Inka Liesmaa, Eira Poikonen, Reetta Kivisaari and Virve Resta are particularly thanked for their contributions.

I want to thank also Helena Kervinen and Antti Kohvakka from Malmi Hospital, as they have taught me almost everything I know about clinical cardiology and echocardiography. I also thank Docent Marju Tilly-Kiesi for encouraging me to make changes in my life and to go on with radiology and science. Markku Vornanen, from Töölö Hospital, I thank for performing an exellent operation on my back on April 2004.

I warmly thank Professor Leena Laasonen, Docent Pekka Tervahartiala, Kirsti Numminen, Marina Rosliakova and all personnel in Department of Radiology at the Surgical Hospital for their patience. I also thank Outi Sipilä for helping me to study MRI physics, in addition Marja Riihimäki and Helena Lustig for their help. I am grateful to technicians Aki Syrjälä and Timo Päivärinta for performing the MR studies.

My deep gratitude goes to my parents Marjatta and Otto Kokki and Professor Anna-Kaisa Järvinen and Matti Järvinen for consistent support.

My special, loving and caring thanks are due to my "boys". My dear husband and closest friend Jussi has supported me during this work and has contributed to most important project: my son Jaakko. Jaakko has also been so patient as he can!

These thesis has been partly financed by a grant from the Helsinki University Central Hospital Research Fund, the Radiology Society of Finland, the Pehr Oscar Klingendahl Foundation, the BIOMEDICUM Helsinki Foundation, the Graduate School "Functional Imaging in Medicine" program (Academy of Finland, Ministry of Education), and the Waldemar von Frenckell Foundation.

Helsinki 21.4.2004,

Sari Kivistö

12. REFERENCES

Alfakih, K., Bloomer, T., Bainbridge, S., Bainbridge, G., Ridgway, J., Williams, G. & Sivananthan, M. (2004a) A comparison of left ventricular mass between two-dimensional echocardiography, using fundamental and tissue harmonic imaging, and cardiac MRI in patients with hypertension. *European Journal of Radiology,* **52,** 103-109.

Alfakih, K., Plein, S., Bloomer, T., Jones, T., Ridgway, J. & Sivananthan, M. (2003a) Comparison of right ventricular volume measurements between axial and short axis orientation using steady-state free precession magnetic resonance imaging. *Journal of Magnetic Resonance Imaging,* **18,** 25-32.

Alfakih, K., Plein, S., Thiele, H., Jones, T., Ridgway, J.P. & Sivananthan, M.U. (2003b) Normal human left and right ventricular dimensions for MRI as assessed by turbo gradient echo and steady-state free precession imaging sequences. *Journal of Magnetic Resonance Imaging,* **17,** 323-329.

Alfakih, K., Reid, S., Jones, T. & Sivananthan, M. (2004b) Assessment of ventricular function and mass by cardiac magnetic resonance imaging. *European Radiology,* **14,** 1813-1822.

Allison, J.D., Flickinger, F.W., Wright, J.C., Falls, D.G., Prisant, L.M., VonDohlen, T.W. & Frank, M.J. (1993) Measurement of left ventricular mass in hypertrophic cardiomyopathy using MRI: comparison with echocardiography. *Magnetic Resonance Imaging,* **11,** 329-334.

Andrew, P. (2003) Diastolic heart failure demystified.[see comment]. [Review] [47 refs]. *Chest,* **124,** 744-753.

Aurigemma, G.P. & Gaasch, W.H. (2004) Clinical practice. Diastolic heart failure. [Review] [56 refs]. *New England Journal of Medicine,* **351,** 1097-1105.

Avela, K., Lipsanen-Nyman, M., Idanheimo, N., Seemanova, E., Rosengren, S., Makela, T.P., Perheentupa, J., Chapelle, A.D. & Lehesjoki, A.E. (2000) Gene encoding a new RING-B-box-Coiled-coil protein is mutated in mulibrey nanism. *Nature Genetics,* **25,** 298-301.

Avela, K., Lipsanen-Nyman, M., Perheentupa, J., Wallgren-Pettersson, C., Marchand, S., Faure, S., Sistonen, P., de la Chapelle, A. & Lehesjoki, A.E. (1997) Assignment of the mulibrey nanism gene to 17q by linkage and linkage-disequilibrium analysis. *American Journal of Human Genetics,* **60,** 896-902.

Axel, L. (2004) Assessment of pericardial disease by magnetic resonance and computed tomography. [Review] [11 refs]. *Journal of Magnetic Resonance Imaging,* **19,** 816-826.

Bellenger, N.G., Burgess, M.I., Ray, S.G., Lahiri, A., Coats, A.J., Cleland, J.G. & Pennell, D.J. (2000a) Comparison of left ventricular ejection fraction and volumes in heart failure by echocardiography, radionuclide ventriculography and cardiovascular magnetic resonance; are they interchangeable?[see comment]. *European Heart Journal,* **21,** 1387-1396.

Bellenger, N.G., Francis, J.M., Davies, C.L., Coats, A.J. & Pennell, D.J. (2000b) Establishment of performance of a magnetic resonance cardiac function clinic. *Journal of Cardiovascular Magnetic Resonance,* **2(1),** 15-22.

Bland, J.M. & Altman, D. (1986) Statistical methods for assessing agreement between two methods of clinical measurement. *Lancet,* **1,** 307-310.

Bogaert, J.& Rademakers, F.E. (2001) Regional nonuniformity of normal adult human left ventricle. *American Journal of Physiology Heart & Circulatory Physiology,* **280,** H610-H620.

Bottini, P.B., Carr, A.A., Prisant, L.M., Flickinger, F.W., Allison, J.D. & Gottdiener, J.S. (1995) Magnetic resonance imaging compared to echocardiography to assess left ventricular mass in the hypertensive patient. *American Journal of Hypertension,* **8,** 221-228.

Burkhoff, D., Maurer, M.S. & Packer, M. (2003) Heart failure with a normal ejection fraction: is it really a disorder of diastolic function?[comment]. *Circulation,* **107,** 656-658.

Di Cesare, E. (2001) MRI of the cardiomyopathies. *European Journal of Radiology,* **38,** 179-184.

Dubach, P., Myers, J., Dziekan, G., Goebbels, U., Reinhart, W., Muller, P., Buser, P., Stulz, P., Vogt, P. & Ratti, R. (1997) Effect of high intensity exercise training on central hemodynamic responses to exercise in men with reduced left ventricular function. *Journal of the American College of Cardiology,* **29,** 1591-1598.

Earls, J.P., Ho, V.B., Foo, T.K., Castillo, E. & Flamm, S.D. (2002) Cardiac MRI: recent progress and continued challenges.[erratum appears in J Magn Reson Imaging. 2002 Nov;16(5):620.]. [Review] [169 refs]. *Journal of Magnetic Resonance Imaging,* **16,** 111-127.

Edwards, M.B., Taylor, K.M., Shellock, F.G. & . (2000) Prosthetic heart valves: evaluation of magnetic field interactions, heating, and artifacts at 1.5 T. *Journal of Magnetic Resonance Imaging,* **12,** 363-369.

Ehsani, A.A., Ogawa, T., Miller, T.R., Spina, R.J. & Jilka, S.M. (1991) Exercise training improves left ventricular systolic function in older men. *Circulation,* **83,** 96-103.

Fagard, R. (2003) Athlete's heart. [Review] [20 refs]. *Heart (British Cardiac Society),* **89,** 1455-1461.

Feinstein, J.A., Epstein, F.H., Arai, A.E., Foo, T.K., Hartley, M.R., Balaban, R.S. & Wolff, S.D. (1997) Using cardiac phase to order reconstruction (CAPTOR): a method to improve diastolic images. *Journal of Magnetic Resonance Imaging,* **7,** 794-798.

Finkelhor, R.S., Hanak, L.J. & Bahler, R.C. (1986) Left ventricular filling in endurance-trained subjects. *Journal of the American College of Cardiology,* **8,** 289-293.

Fonseca, C.G., Oxenham, H.C., Cowan, B.R., Occleshaw, C.J. & Young, A.A. (2003) Aging alters patterns of regional nonuniformity in LV strain relaxation: a 3-D MR tissue tagging study. *American Journal of Physiology Heart & Circulatory Physiology,* **285**,H621-H630.

Frank, H. & Globits, S. (1999) Magnetic resonance imaging evaluation of myocardial and pericardial disease. [Review] [52 refs]. *Journal of Magnetic Resonance Imaging,* **10,** 617-626.

Friedrich, M.G. (2000) Magnetic resonance imaging in cardiomyopathies. [Review] [132 refs]. *Journal of Cardiovascular Magnetic Resonance,* **2,** 67-82.

Fujita, N., Hartiala, J., O'Sullivan, M., Steiman, D., Chatterjee, K., Parmley, W.W. & Higgins, C.B. (1993) Assessment of left ventricular diastolic function in dilated cardiomyopathy with cine magnetic resonance imaging: effect of an angiotensin converting enzyme inhibitor, benazepril. *American Heart Journal,* **125,** 171-178.

Garcia, M.J., Thomas, J.D. & Klein, A.L. (1998) New doppler echocardiographic applications for the study of diastolic function. *Journal of the American College of Cardiology,* **32,** 865-975.

Gibson, D.G. & Francis, D.P. (2003) Clinical assessment of left ventricular diastolic function.[see comment]. [Review] [31 refs]. *Heart,* **89,** 231-238.

Gledhill, N., Cox, D. & Jamnik, R. (1994) Endurance athletes' stroke volume does not plateau: major advantage is diastolic function. *Medicine & Science in Sports & Exercise,* **26,** 1116-1121.

Graves, M.J., Berry, E., Eng, A.A., Westhead, M., Black, R.T., Beacock, D.J., Kelly, S. & Niemi, P. (2000) A multicenter validation of an active contour-based left ventricular analysis technique. *Journal of Magnetic Resonance Imaging,* **12,** 232-239.

Greenberg, S.B. & Sandhu, S.K. (1999) Ventricular function. [Review] [93 refs]. *Radiologic Clinics of North America,* **37,** 341-359, vi.

Haase, A. (1990) Snapshot FLASH MRI. Applications to T1, T2, and chemical-shift imaging. *Magnetic Resonance in Medicine,* **13,** 77-89.

Hartiala, J.J., Foster, E., Fujita, N., Mostbeck, G.H., Caputo, G.R., Fazio, G.P., Winslow, T. & Higgins, C.B. (1994) Evaluation of left atrial contribution to left ventricular filling in aortic stenosis by velocity-encoded cine MRI. *American Heart Journal,* **127,** 593-600.

Hartiala, J.J., Mostbeck, G.H., Foster, E., Fujita, N., Dulce, M.C., Chazouilleres, A.F. & Higgins, C.B. (1993) Velocity-encoded cine MRI in the evaluation of left ventricular diastolic function: measurement of mitral valve and pulmonary vein flow velocities and flow volume across the mitral valve. *American Heart Journal,* **125,** 1054-1066.

Hartnell, G.G., Hughes, L.A., Ko, J.P. & Cohen, M.C. (1996) Magnetic resonance imaging of pericardial constriction: comparison of cine MR angiography and spin-echo techniques. *Clinical Radiology,* **51,** 268-272.

Hatle, L. & Sutherland, G.R. (2000) Regional myocardial function--a new approach. *European Heart Journal,* **21,** 1337-1357.

Henriksen, E., Landelius, J., Kangro, T., Jonason, T., Hedberg, P., Wesslen, L., Rosander, C.N., Rolf, C., Ringqvist, I. & Friman, G. (1999) An echocardiographic study of right and left ventricular adaptation to physical exercise in elite female orienteers. *European Heart Journal,* **20,** 309-316.

Higgins, C.B. (2000) Cardiac imaging.[see comment]. [Review] [26 refs]. *Radiology,* **217,** 4-10.
Juergens, K.U., Grude, M., Maintz, D., Fallenberg, E.M., Wichter, T., Heindel, W. & Fischbach, R. (2004) Multi-Detector Row CT of left ventricular function with dedicated analysis software versus MR imaging: Initial experience. *Radiology,* **230,** 403-410.

Järvinen, V., Kupari, M., Hekali, P. & Poutanen, V.P. (1994a) Assessment of left atrial volumes and phasic function using cine magnetic resonance imaging in normal subjects. *American Journal of Cardiology,* **73,** 1135-1138.

Järvinen, V.M., Kupari, M.M., Hekali, P.E. & Poutanen, V.P. (1994b) Right atrial MR imaging studies of cadaveric atrial casts and comparison with right and left atrial volumes and function in healthy subjects. *Radiology,* **191,** 137-142.

Jääskelainen, P., Miettinen, R., Karkkainen, P., Toivonen, L., Laakso, M. & Kuusisto, J. (2004) Genetics of hypertrophic cardiomyopathy in eastern Finland: few founder mutations with benign or intermediary phenotypes. [Review] [39 refs]. *Annals of Medicine,* **36,** 23-32.

Katz, J., Milliken, M.C., Stray-Gundersen, J., Buja, L.M., Parkey, R.W., Mitchell, J.H. & Peshock, R.M. (1988) Estimation of human myocardial mass with MR imaging. *Radiology,* **169,** 495-498.

Kitzman, D.W., Little, W.C., Brubaker, P.H., Anderson, R.T., Hundley, W.G., Marburger, C.T., Brosnihan, B., Morgan, T.M. & Stewart, K.P. (2002) Pathophysiological characterization of isolated diastolic heart failure in comparison to systolic heart failure. *Journal of the American Medical Association,* **288,** 2144-2150.

Kojima, S., Yamada, N. & Goto, Y. (1999) Diagnosis of constrictive pericarditis by tagged cine magnetic resonance imaging. *New England Journal of Medicine,* **341,** 373-374.

Kozerke, S., Tsao, J., Razavi, R. & Boesiger, P. (2004) Accelerating cardiac cine 3D imaging using k-t BLAST. *Magnetic Resonance in Medicine,* **52,** 19-26.

Kramer, C.M., Reichek, N., Ferrari, V.A., Theobald, T., Dawson, J. & Axel, L. (1994) Regional heterogeneity of function in hypertrophic cardiomyopathy. *Circulation,* **90,** 186-194.

Kroft, L.J., Simons, P., van Laar, J.M. & de Roos, A. (2000) Patients with pulmonary fibrosis: cardiac function assessed with MR imaging. *Radiology,* **216,** 464-471.

Krombach, G.A., Saeed, M. & Higgins, C.B. (2002) Myocardial and pericardial diseases In *Cardiovascular MRI & MRA* (Higgins, C.B. & de Roos, A. eds.), pp. 104-121. Lippincott Williams &Wilkins.

Kudelka, A.M., Turner, D.A., Liebson, P.R., Macioch, J.E., Wang, J.Z. & Barron, J.T. (1997) Comparison of cine magnetic resonance imaging and Doppler echocardiography for evaluation of left ventricular diastolic function. *American Journal of Cardiology,* **80,** 384-386.

Kuhl, H.P., Spuentrup, E., Wall, A., Franke, A., Schröder, J., Heussen, N., Hanrath, P., Gunther, R.W. & Buecker, A. (2004) Assessment of myocardial function with interactive non-breath-hold real-time MR imaging: comparison with echocardiography and breath-hold Cine MR imaging. *Radiology,* **231,** 198-207.

Levine, B.D., Lane, L.D., Buckey, J.C. & D.B., F. (1991) Left ventricular pressure-volume and frank-starling relations in endurance athletes. Implications for ortostatis tolerance and exercise performance. *Circulation,* **84,** 1016-1023.

Levy, W.C., Cerqueira, M.D., Abrass, I.B., Schwartz, R.S. & Stratton, J.R. (1993) Endurance exercise training augments diastolic filling at rest and during exercise in healthy young and older men. *Circulation,* **88,** 116-126.

Libonati, J.R. (2000) Exercise training improves left ventricular isovolumic relaxation. *Medicine & Science in Sports & Exercise,* **32,** 1399-1405.

Libonati, J.R., Colby, A.M., Caldwell, T.M., Kasparian, R. & Glassberg, H.L. (1999) Systolic and diastolic cardiac function time intervals and exercise capacity in women. *Medicine & Science in Sports & Exercise,* **31,** 258-263.

Lipsanen-Nyman, M., Perheentupa, J., Rapola, J., Sovijarvi, A. & Kupari, M. (2003) Mulibrey heart disease: clinical manifestations, long-term course, and results of pericardiectomy in a series of 49 patients born before 1985. *Circulation.,* **107,** 2810-2815.

Lipton, M.J. & Coulden, R. (1999) Valvular heart disease. [Review] [34 refs]. *Radiologic Clinics of North America,* **37,** 319-339, v-vi.

Lorenz, C.H., Flacke, S. & Fischer, S.E. (2000) Noninvasive modalities. Cardiac MR imaging. [Review] [65 refs]. *Cardiology Clinics,* **18,** 557-570.

Lorenz, C.H., Walker, E.S., Morgan, V.L., Klein, S.S. & Graham, T.P., Jr. (1999) Normal human right and left ventricular mass, systolic function, and gender differences by cine magnetic resonance imaging. *Journal of Cardiovascular Magnetic Resonance,* **1,** 7-21.

Lorenzo-Valdes´, M., Sanchez-Ortiz, G.I., Elkington, A.G., Mohiaddin, R.H. & Rueckert, D. (2004) Segmentation of 4D cardiac images using a probabilistic atlas and the EM algorithm. *Medical Image Analysis,* **8,** 255-265.

Lötjönen, J. (2003a) Construction of patient-specific surface models from MR images: application to bioelectromagnetism. *Computer Methods & Programs in Biomedicine,* **72,** 167-178.

Lötjönen, J., Kivistö, S., Koikkalainen, J., Smutek, D., Lauerma, K. (2004a) Statisistical shape model of atria, ventricles and epicardium from short- and lon-axis MR images. *Medical Image Analysis,* **8,** 371-386.

Lötjönen, J., Koikkalainen, J., Smutek., D., Kivistö, S. & Lauerma, K. (2003) Four-camber statistical 3-D heart model from short-axis and long-axis MR images. *Lecture notes in computer science,* **2878,** 459-466.

Lötjönen, J., Pollari, M., Kivistö, S., Lauerma, K. (2004b) Correction of movement artifacts from 4-D cardiac short- and long-axis data. *Lecture notes in computer science,* **3217,** 427-434, Part 422.

Lötjönen, J., Smutek, D., Kivistö, S., Lauerma, K. (2003b) Tracking atrial and ventricles simultaneously from cardiac short-and long-axis MR images. *Lecture notes in computer science,* **2878,** 467-474.

Mandinov, L., Eberli, F.R., Seiler, C. & Hess, O.M. (2000) Diastolic heart failure. [Review] [75 refs]. *Cardiovascular Research,* **45,** 813-825.

Marcus, J.T., DeWaal, L.K., Gotte, M.J., van der Geest, R.J., Heethaar, R.M. & Van Rossum, A.C. (1999) MRI-derived left ventricular function parameters and mass in healthy young adults: relation with gender and body size. *International Journal of Cardiac Imaging,* **15,** 411-419.

Masood, S., Yang, G.-Z., Pennell, D.J. & Firmin, D.N. (2000) Investigating intrinsic myocardial mechanics: The role of MR tagging, velocity phase mapping, and diffusion imaging. *Journal of Magnetic Resonance Imaging,* **12,** 873-883.

Masui, T., Finck, S. & Higgins, C.B. (1992) Constrictive pericarditis and restrictive cardiomyopathy: evaluation with MR imaging. *Radiology,* **182,** 369-373.

Matsuda, M., Sugishita, Y., Koseki, S., Ito, I., Akatsuka, T. & Takamatsu, K. (1983) Effect of exercise on left ventricular diastolic filling in athletes and nonathletes. *Journal of Applied Physiology: Respiratory, Environmental & Exercise Physiology,* **55,** 323-328.

Milliken, M.C., Stray-Gundersen, J., Peshock, R.M., Katz, J. & Mitchell, J.H. (1988) Left ventricular mass as determined by magnetic resonance imaging in male endurance athletes. *American Journal of Cardiology.,* **62,** 301-305.

Mitchell, S.C., Bosch, J.G., Lelieveldt, B.P., van der Geest, R.J., Reiber, J.H. & Sonka, M. (2002) 3-D active appearance models: segmentation of cardiac MR and ultrasound images. *IEEE Transactions on Medical Imaging,* **21,** 1167-1178.

Moon, J.C., Lorenz, C.H., Francis, J.M., Smith, G.C. & Pennell, D.J. (2002) Breath-hold FLASH and FISP cardiovascular MR imaging: left ventricular volume differences and reproducibility. *Radiology,* **223,** 789-797.

Myers, J., Wagner, D., Schertler, T., Beer, M., Luchinger, R., Klein, M., Rickli, H., Muller, P., Mayer, K., Schwitter, J. & Dubach, P. (2002) Effects of exercise training on left ventricular volumes and function in patients with nonischemic cardiomyopathy: application of magnetic resonance myocardial tagging. *American Heart Journal,* **144,** 719-725.

Myerson, S.G., Bellenger, N.G. & Pennell, D.J. (2002) Assessment of left ventricular mass by cardiovascular magnetic resonance. *Hypertension,* **39,** 750-755.

Nagueh, S.F., McFalls, J., Meyer, D., Hill, R., Zoghbi, W.A., Tam, J.W., Quinones, M.A., Roberts, R. & Marian, A.J. (2003) Tissue doppler imaging predicts the development of hypertrophic cardiomyopathy in subjects with sublinical disease. *Circulation,* **108,** 395-398.

Nitz, W. (1999) Principles of magnetic resonance imaging and magnetic resonance angiography In *A Practical Approach Clinical MR Imaging* (Reimer Peter, P.P.M., Stichnoth Falko-A. ed.), pp. 1-35. Springer-Verlag Berlin Heidelberg New York, Germany.

Nixon, J.V., Wright, A.R., Porter, T.R., Roy, V. & Arrowood, J.A. (1991) Effects of exercise on left ventricular diastolic performance in trained athletes. *American Journal of Cardiology,* **68,** 945-949.

Nottin, S., Nguyen, L.-D., Terbah, M., Obert, P. (2004) Long-term endurance tarining does not prevent the age-related decrease in left ventricular relaxation properties. *Acta Physiologica Scandinavica,* **181,** 209-215.

Ommen, S.R., Nishimura, R.A., Appleton, C.P., Miller, F.A., Oh, J.K., Redfield, M.M. & Tajik, A.J. (2000) Clinical utility of doppler echocardiography and tissue doppler imaging in the estimation of left ventricular fillinf pressures. A comparative simultaneous doppler-catheterization study. *Circulation,* **102,** 1788-1794.

Otto, C.A. & Pearlman, A.S. (1995) Pericardial disease: two-dimensional echocardiographic and doppler findings In *Textbook of clinical echocardiography*, pp. 193-208. W.S. Saunders Company, Philadelphia.

Otto, C.A., Pearlman, A.S. (1995) Echocardiographic evaluation of ventricular diastolic fiolling and function In *Textbook of clinical echocardiocraphy*, pp. 117-136. W.B. Saunders Company, Philadelphia.

Owen, A., Theakston, Simon C., O´Donovan, Gary, Bird, Steve R. (2004) Right and left ventricular diastolic function of male endurance athletes. *International Journal of Cardiology,* **95,** 231-235.

Paelinck, B.P., Lamb, H.J., Bax, J.J., Van der Wall, E.E. & de Roos, A. (2002) Assessment of diastolic function by cardiovascular magnetic resonance. [Review] [46 refs]. *American Heart Journal,* **144,** 198-205.

Palka, P., Lange, A. & Nihoyannopoulos, P. (1999) The effect of long-term training on age-related left ventricular changes by Doppler myocardial velocity gradient. *American Journal of Cardiology,* **84,** 1061-1067.

Pattynama, P.M., de Roos, A., Van der Wall, E.E. & Van Voorthuisen, E. (1994) Evaluation of cardiac function with magnetic resonance imaging. *American Heart Journal,* **128,** 595-607.

Pattynama, P.M., Lamb, H.J., Van der Velde, E.A., Van der Geest, R.J., Van der Wall, E.E. & De Roos, A. (1995) Reproducibility of MRI-derived measurements of right ventricular volumes and myocardial mass. *Magnetic Resonance Imaging,* **13,** 53-63.

Pattynama, P.M., Lamb, H.J., van der Velde, E.A., van der Wall, E.E. & de Roos, A. (1993) Left ventricular measurements with cine and spin-echo MR imaging: a study of reproducibility with variance component analysis. *Radiology,* **187,** 261-268.

Pennell, D.J. (2002) Ventricular volume and mass by CMR. *Journal of Cardiovascular Magnetic Resonance,* **4,** 507-513.

Perheentupa, J., Autio, S., Leisti, S., Raitta,C., Tuuteri L. (1973) Mulibrey nanism, an autosomal recessive syndrome with pericardial constriction. *Lancet,* **2,** 351-355.

Pettigrew, R.I., Oshinski, J.N., Chatzimavroudis, G. & Dixon, W.T. (1999) MRI techniques for cardiovascular imaging. [Review] [39 refs]. *Journal of Magnetic Resonance Imaging,* **10,** 590-601.

Pluim, B.M., Beyerbacht, H.P., Chin, J.C., Zwinderman, A., Van der Laarse, A., De Roos, A., Vliegen, H.W. & Van der Wall, E.E. (1997) Comparison of echocardiography with magnetic resonance imaging in the assessment of the athlete's heart. *European Heart Journal,* **18,** 1505-1513.

Pluim, B.M., Lamb, H.J., Kayser, H.W., Leujes, F., Beyerbacht, H.P., Zwinderman, A.H., van der Laarse, A., Vliegen, H.W., de Roos, A. & van der Wall, E.E. (1998) Functional and metabolic evaluation of the athlete's heart by magnetic resonance imaging and dobutamine stress magnetic resonance spectroscopy. *Circulation,* **97,** 666-672.

Pluim, B.M., Zwinderman, A.H., van der Laarse, A. & van der Wall, E.E. (2000) The athlete's heart. A meta-analysis of cardiac structure and function.[see comment]. *Circulation,* **101,** 336-344.

Redfield, M.M. (1930) Understanding "diastolic" heart failure.[see comment][comment]. *New England Journal of Medicine,* **350,** 1930-1931.

Redfield, M.M., Jacobsen, S.J., Burnett, J.C., Jr., Mahoney, D.W., Bailey, K.R. & Rodeheffer, R.J. (2003) Burden of systolic and diastolic ventricular dysfunction in the community: appreciating the scope of the heart failure epidemic.[see comment]. *Journal of the American Medical Association,* **289,** 194-202.

Rehr, R.B., Malloy, C.R., Filipchuk, N.G. & Peshock, R.M. (1985) Left ventricular volumes measured by MR imaging. *Radiology,* **156,** 717-719.

Reichek, N. (1999) MRI myocardial tagging. [Review] [41 refs]. *Journal of Magnetic Resonance Imaging,* **10,** 609-616.

Rumberger, J.A., Lipton, M.J. (1989) Ultrafast cardiac CT scanning. *Cardiology Clinics,* **7,** 713-734.

Scharhag, J., Schneider, G., Urhausen, A., Rochette, V., Kramann, B. & Kindermann, W. (2002) Athlete's heart: right and left ventricular mass and function in male endurance athletes and untrained individuals determined by magnetic resonance imaging. *Journal of the American College of Cardiology,* **40,** 1856-1863.

Semelka, R.C., Tomei, E., Wagner, S., Mayo, J., Caputo, G., O'Sullivan, M., Parmley, W.W., Chatterjee, K., Wolfe, C. & Higgins, C.B. (1990) Interstudy reproducibility of dimensional and functional measurements between cine magnetic resonance studies in the morphologically abnormal left ventricle. *American Heart Journal,* **119,** 1367-1373.

Shaphiro, L.M. & Smith, R.G. (1983) Effect of training on left ventricular structure and function: an echocardiographic study. *Brithish Heart Journal,* **50,** 534-539.

Sievers, B., Addo, M., Franken, U. & Trappe, H.-J. (2004) Right ventricular wall motion abnormalities found in healthy subjects by cardiovascular magnetic resonance imaging and characterized with a new segmentation model. *Journal of Cardiovascular Magnetic Resonance,* **6,** 601-608.

Sipola, P., Lauerma, K., Husso-Saastamoinen, M., Kuikka, J.T., Vanninen, E., Laitinen, T., Manninen, H., Niemi, P., Peuhkurinen, K., Jaaskelainen, P., Laakso, M., Kuusisto, J. & Aronen, H.J. (2003a) First-pass MR imaging in the assessment of perfusion impairment in patients with

hypertrophic cardiomyopathy and the Asp175Asn mutation of the alpha-tropomyosin gene. *Radiology,* **226,** 129-137.

Sipola, P., Vanninen, E., Aronen, H.J., Lauerma, K., Simula, S., Jaaskelainen, P., Laakso, M., Peuhkurinen, K., Kuusisto, J. & Kuikka, J.T. (2003b) Cardiac adrenergic activity is associated with left ventricular hypertrophy in genetically homogeneous subjects with hypertrophic cardiomyopathy. *Journal of Nuclear Medicine,* **44,** 487-493.

Soldo, S.J., Norris, S.L., Gober, J.R., Haywood, L.J., Colletti, P.M. & Terk, M. (1994) MRI-derived ventricular volume curves for the assessment of left ventricular function. *Magnetic Resonance Imaging,* **12,** 711-717.

Sondergaard, L., Stahlberg, F. & Thomsen, C. (1999) Magnetic resonance imaging of valvular heart disease. [Review] [125 refs]. *Journal of Magnetic Resonance Imaging,* **10,** 627-638.

Soulen, R.L. (1991) Magnetic resonance imaging of great vessel, myocardial, and pericardial disease. *Circulation,* **84,** I311-321.

Sprung, K. (2005) Basic techniques of cardiac MR. *European Radiology,* **15(Suppl 2),** B10-B16.

Stark, D.D., Higgins, C.B., Lanzer, P., Lipton, M.J., Schiller, N., Crooks, L.E., Botvinick, E.B. & Kaufman, L. (1984) Magnetic resonance imaging of the pericardium: normal and pathologic findings. *Radiology,* **150,** 469-474.

Szolar, D.H., Sakuma, H. & Higgins, C.B. (1996) Cardiovascular applications of magnetic resonance flow and velocity measurements. [Review] [95 refs]. *Journal of Magnetic Resonance Imaging,* **6,** 78-89.

Takemoto, K.A., Bernstein, L., Lopez, J.F., Marshak, D., Rahimtoola, S.H. & Chandraratna, P.A. (1992) Abnormalities of diastolic filling of the left ventricle associated with aging are less pronounced in exercise-trained individuals. *American Heart Journal,* **124,** 143-148.

Tsutsui, H., Tsuchihashi, Miyuki, Takeshita, Akira (2001) Mortality and readmission of hospitalized patients with congestive heart failure and preserved versus depressed systolic function. *The American Journal of Cardiology,* **88,** 530-533.

Tuuteri, L., Perheentupa, J. & Rapola, J. (1974) The cardiopathy of mulibrey nanism, a new inherited syndrome. *Chest,* **65,** 628-631.

van der Geest, R.J., Buller, V.G., Jansen, E., Lamb, H.J., Baur, L.H., van der Wall, E.E., de Roos, A. & Reiber, J.H. (1997) Comparison between manual and semiautomated analysis of left ventricular volume parameters from short-axis MR images. *Journal of Computer Assisted Tomography,* **21,** 756-765.

van der Geest, R.J., Lelieveldt, B.P.F., Angelie, E., Danilouchkine, M., Swingen, C., Sonka, M. & Reiber, J.H. (2004) Evaluation of a new method for automated detection of left ventricular boundaries in time series of magnetic resonance images using an active appearance motion model. *Journal of Cardiovascular Magnetic Resonance,* **6,** 609-617.

Warner, J.G., Jr., Metzger, D.C., Kitzman, D.W., Wesley, D.J. & Little, W.C. (1999) Losartan improves exercise tolerance in patients with diastolic dysfunction and a hypertensive response to exercise. *Journal of the American College of Cardiology,* **33,** 1567-1572.

Wernstedt, P., Sjostedt, C., Ekman, I., Du, H., Thuomas, K.A., Areskog, N.H. & Nylander, E. (2002) Adaptation of cardiac morphology and function to endurance and strength training. A comparative study using MR imaging and echocardiography in males and females. *Scandinavian Journal of Medicine & Science in Sports,* **12,** 17-25.

Westbrook, C. & Kaut, C. (1995) Basic principles In *MRI in Practise* (Westbrook, C. & Kaut, C. eds.), pp. 1-16. Blackwell science, Oxford.

Zile, M.R., Baicu, C.F. & Gaasch, W.H. (2004) Diastolic heart failure--abnormalities in active relaxation and passive stiffness of the left ventricle.[see comment]. *New England Journal of Medicine,* **350,** 1953-1959.

Zile, M.R. & Brutsaert, D.L. (2002a) New concepts in diastolic dysfunction and diastolic heart failure: Part I: diagnosis, prognosis, and measurements of diastolic function. [Review] [53 refs]. *Circulation,* **105,** 1387-1393.

Zile, M.R. & Brutsaert, D.L. (2002b) New concepts in diastolic dysfunction and diastolic heart failure: Part II: causal mechanisms and treatment. [Review] [53 refs]. *Circulation,* **105,** 1503-1508.